Available online at www.sciencedirect.com
ScienceDirect
Comput. Methods Appl. Mech. Engrg. 393 (2022) 114736
Computer methods in applied mechanics and engineering
www.elsevier.com/locate/cma

Efficient computation of time-periodic compressible flows with spectral techniques

Javier Sierra-Ausin[a,b], Vincenzo Citro[a,*], Flavio Giannetti[a], David Fabre[b]

[a] DIIN, Via Giovanni Paolo II, 132, 84084 Fisciano SA, Italy
[b] IMFT, 2 Allé du Professeur Camille Soula, 31400 Toulouse, France

Received 3 May 2021; received in revised form 17 September 2021; accepted 5 February 2022
Available online 24 February 2022

Abstract

A systematic approach to parametrically analyze compressible time-periodic flows is proposed. Instead of time-stepping simulations, a Fourier–Galerkin strategy is adopted, which consists of the projection of the periodic solution onto a truncated Fourier series. Starting from the compressible Navier–Stokes equations, a truncated nonlinear problem coupling the $2N + 1$ fields, representing the Fourier discretization, is derived. This nonlinear problem is solved by Newton iteration and a set of efficient algorithms for the resolution of the arising inner linear systems is proposed. Compared to alternative methods, the formulation is free of any numerical constraint affecting performance, e.g. a CFL-like condition. It is also free of aliasing effects arising in other spectral techniques. The efficiency of the method is illustrated for two configurations where sound is radiated due to a flow instability, namely the flow around a circular cylinder and the flow through two successive apertures, i.e. the hole-tone configuration.

Keywords: Spectral method; Acoustics; Compressible flows; Nonlinear dynamics; Limit cycle

1. Introduction

Many fluid dynamics problems are characterized by the spontaneous emergence of time-periodic solutions. The classical approach in the studying of periodic states is to perform time integration of the governing equations up to convergence to a stable (unstable) limit cycle. However, this approach can become rapidly very expensive in some circumstances. For instance, it is notably inefficient near bifurcations leading to unsteadiness where transients can be lengthy. It is also unsuited to cases where the underlying physics imposes tiny time steps. This situation is met for example with compressible, low-Mach-number limit flows involving acoustic radiation, where a severe time-step restriction is imposed by the large separation in convective and acoustic velocity scales.

Several ideas have been proposed to speed-up the convergence of time-stepping towards a limit cycle, for instance, using time filters [1] or considering symmetries [2]. However, the efficiency of such approaches remains case-dependent. An alternative idea is to take advantage of the time periodicity of the expected solution by applying

* Corresponding author.
E-mail address: vcitro@unisa.it (V. Citro).

https://doi.org/10.1016/j.cma.2022.114736
0045-7825/

spectral techniques to the time discretization and directly solving for the entire cycle. The problem may be worked out either in spectral or time domain, leading to two distinct classes of methods.

In the first case, formulating the problem in the spectral domain leads to the Harmonic Balance (or Fourier–Galerkin) formulation, a representation of the cycle by a truncated Fourier series up to Nth order. The Navier–Stokes equations are then written in spectral space, leading to a system coupling the $2N + 1$ Fourier components. This last system can be solved globally using, for instance, a Newton iteration. This method is useful for the study of low-dimensional systems of equations modeling mechanical problems [3]. Recently, an alternative formulation of the Harmonic-Balance called *self-consistent method* has been introduced for order $N = 1$ [4,5] and subsequently adapted to order $N = 2$ [6]. Self-consistent method has gained some popularity in the fluid instability community (see [7] for a discussion on the link between harmonic-balance and self-consistent method). Besides a description of the limit cycle, the *self-consistent method* yields an amplitude equation describing the transient dynamics towards it. A generalization of the method to compressible flows was proposed by [8] for the wake of a cylinder. However, the accuracy of the truncation to order $N = 1$ remains case-dependent. A general implementation of the Harmonic Balance method in frequency domain for compressible flows up to arbitrary order N is still missing.

Alternatively, the problem may be formulated in time, leading to the so called time-spectral method. In this case, the $2N + 1$ Fourier components are replaced by $2N + 1$ "snapshots" representing the cycle. The equations are evaluated in the time domain, but the time-derivative is computed in the frequency domain, thus requiring direct and inverse discrete Fourier transforms to pull back this term into the time domain. Time Spectral Method has been successfully used for the characterization of high Reynolds flows in the field of turbomachinery, e.g. Hall et al. [9] and Mavriplis et al. [10], where it is considered as a closure model of averaged equations, or an alternative to Unsteady Reynolds Averaged Navier–Stokes equations (URANS) (see Ekici et al. [11], Sicot et al. [12] and references therein). Recently, it has been extended for the treatment of free-surface flows and fluid structure interaction problems (see Gatin et al. [13] and Yao et al. [14]).

Despite their limited usage in the literature, the Fourier–Galerkin formulation presents a series of advantages regarding other approaches requiring the action of the discrete Fourier transform cf. [15]. First, the approach is free of aliasing errors because the projection onto the Fourier basis is analytical, i.e. it evaluates the analytical Fourier coefficients of the residual. On the contrary, Time-Spectral-Method (TSM) and other similar methodologies rely on sampling a series of time-instants and on the use of successive discrete Fourier transforms, which if in one hand may permit faster evaluations of the residual in case of strong nonlinearity on the other it will inherently add aliasing errors. Under the sampling theorem, higher harmonics of nonlinear terms cannot be resolved with the same number of samples used for linear terms. As a result, methods relying on the discrete Fourier transform must increase the number of degrees of freedom, e.g. the 3/2-rule of Orszag for quadratic nonlinearity [16].

Furthermore, the solution of the TSM formulation may be solved by a fixed-point algorithm, e.g. Newton method or by a pseudo-time marching strategy. In fluid mechanics, in particular for turbomachinery applications, a pseudo-time marching is the preferred strategy to compute the final periodic solution. This strategy is effective at moderate Mach numbers. Nonetheless, at low-Mach-number, where there is a large scale difference between the convective and the acoustic scale, the pseudo-time step must be considerably constrained.

An upper bound for the pseudo-time step is determined from quantities in the acoustic scale either because of CFL or accuracy condition. Regarding the linear stability condition efforts have been paid to enlarge the stability limit: optimal explicit Runge Kutta (ERK) schemes have been determined for several spatial discretization. Examples can be found in the works by Parsani et al. [17] for spectral differences, Citro et al. for classical finite element [18] and Kubatko et al. [19] for discontinuous Galerkin. Nevertheless, the integration of Navier–Stokes equations, even with optimal ERK schemes, requires a significant number of iterations, which makes a full parametric study of low Mach number flows an impractical task.

The aim of the present study is to propose a numerical resolution algorithm for the Fourier–Galerkin method considering an arbitrary truncation order N, allowing an efficient reconstruction of periodic solutions of the compressible Navier–Stokes equations. Governing equations and linear stability are introduced in Section 2. Fourier–Galerkin approach is introduced in Section 3, where particular emphasis is placed on the derivation of nonlinear terms of the Fourier–Galerkin residual (a detailed derivation can be found in Appendix). The resulting nonlinear problem is solved via a Newton–Krylov approach with an efficient preconditioning strategy in a parallel context. Finally, in Section 4 and Section 5 the presented approach is applied to two numerical examples: the flow past a circular cylinder and the sound generation in a hole tone configuration, both in the low-Mach-number limit. In Section 5.1.2 a comparison of the performance of the current implementation of Fourier–Galerkin with TSM is reported for the cylinder case at several Mach numbers.

2. Theoretical formulation

Let us consider the description of nonlinear saturated states of compressible flows. The exposition is sufficiently general to be extended for the study of other type of flows. Nevertheless, attention will be paid to the Fourier–Galerkin representation of the quadratic and cubic nonlinearity.

2.1. Governing equations

Let us consider a compressible fluid motion of a perfect gas (characterized by its specific constant R_g and adiabatic index γ) with constant dynamic viscosity μ and heat conductivity κ. The flow is described by the fluid density $\tilde{\rho}$, the velocity vector field $\tilde{\mathbf{u}} = (\tilde{u}, \tilde{v}, \tilde{w})$, the pressure $\tilde{p}$, and temperature $\tilde{T}$. These dimensional primitive variables are made dimensionless as follows:

$$\mathbf{x} = \frac{\tilde{\mathbf{x}}}{\bar{\ell}}, \quad t = \frac{\tilde{t}\bar{u}}{\bar{\ell}}, \quad \rho = \frac{\tilde{\rho}}{\bar{\rho}}, \quad \mathbf{u} = \frac{\tilde{\mathbf{u}}}{\bar{u}}, \quad T = \frac{\tilde{T}}{\bar{T}}, \quad p = \frac{\tilde{p}}{\bar{\rho}\bar{R}_g\bar{T}}, \tag{1}$$

where reference values are designated by an upper bar $\bar{\cdot}$.

After a convenient choice of the reference length $\bar{\ell}$ and velocity $\bar{u}$, one can classically define three nondimensional numbers (Reynolds, Mach and Prandtl) as follows:

$$Re = \frac{\bar{\rho}\bar{u}\bar{\ell}}{\bar{\mu}}, \quad M = \frac{\bar{u}}{\sqrt{\bar{\rho}\bar{R}_g\bar{T}}}, \quad Pr = \frac{\bar{\mu}}{\bar{\rho}\bar{\kappa}}. \tag{2}$$

Introducing these notations into the compressible Navier–Stokes equations leads to a set of equations governing the evolution of the nondimensional state vector $\mathbf{q} = [\rho, \mathbf{u}, T, p]$. To facilitate the analysis and enlighten the nature of the nonlinearities, it is convenient to write these equations as follows:

$$\mathcal{NS}(\mathbf{q}) \equiv \mathbf{M}\left(\frac{\partial \mathbf{q}}{\partial t}\right) + \mathbf{L}(\mathbf{q}) + \mathbf{F}_2(\mathbf{q}, \mathbf{q}) + \mathbf{F}_3(\mathbf{q}, \mathbf{q}, \mathbf{q}) = \mathbf{0}. \tag{3}$$

In Eq. (3), the "mass" matrix $\mathbf{M}$ multiplying the time-derivative and the linear operator $\mathbf{L}$ are defined as:

$$\mathbf{M} = \begin{pmatrix} 1 & 0 & 0 & 0 \\ 0 & \rho\mathbf{I} & 0 & 0 \\ 0 & 0 & \rho & 0 \\ 0 & 0 & 0 & 0 \end{pmatrix}, \quad \mathbf{L} = \begin{pmatrix} 0 & 0 & 0 & 0 \\ 0 & -\nabla\cdot\tau(\cdot) & 0 & \frac{1}{\gamma M^2}\nabla \\ 0 & 0 & -\frac{\gamma}{Pr}\nabla^2 & 0 \\ 0 & 0 & 0 & 1 \end{pmatrix} \tag{4}$$

The nonlinear terms involve a quadratic operator $\mathbf{F}_2$ and a cubic operator $\mathbf{F}_3$ defined as:

$$\mathbf{F}_2(\mathbf{q}_i, \mathbf{q}_j) = \begin{pmatrix} \mathbf{u}_i\cdot\nabla\rho_j + \rho_i\nabla\cdot\mathbf{u}_j \\ \mathbf{0} \\ (\gamma-1)\Big[p_i\nabla\cdot\mathbf{u}_j - \gamma M^2\tau(\mathbf{u}_i):\mathbf{D}(\mathbf{u}_j)\Big] \\ -\rho_i T_j \end{pmatrix} \tag{5}$$

$$\mathbf{F}_3(\mathbf{q}_i, \mathbf{q}_j, \mathbf{q}_\ell) = \begin{pmatrix} 0 \\ \rho_i\mathbf{u}_j\cdot\nabla\mathbf{u}_\ell \\ \rho_i\mathbf{u}_j\cdot\nabla T_\ell \\ 0 \end{pmatrix} \tag{6}$$

In these expressions, $\mathbf{I}$ denotes the identity operator, whose dimension is determined by the number of velocity components; $\tau(\mathbf{u})$ is the shear stress tensor $\tau(\mathbf{u}) = \frac{1}{Re}\Big[2\mathbf{D}(\mathbf{u}) - \frac{2}{3}(\nabla\cdot\mathbf{u})\mathbf{I}\Big]$ and $\mathbf{D}(\mathbf{u}) = \frac{1}{2}\Big[\nabla\mathbf{u} + \nabla\mathbf{u}^T\Big]$ is the strain tensor. Additionally a set of boundary conditions are needed to close the problem. Specific boundary conditions are case dependent and they are not here specified.

It is important to remark that, unlike incompressible flows where only quadratic nonlinearities are present, compressible Navier–Stokes equations contain both quadratic and cubic nonlinearities. In particular, the term $\rho\mathbf{u}\cdot\nabla\mathbf{u}$, which for incompressible equations is the only nonlinearity and a quadratic one, becomes a cubic nonlinearity in the compressible case. This point explains why a derivation of equations in Fourier–Galerkin method is much more intricate.

To facilitate derivations in following sections, it is convenient to define symmetric nonlinear operators:

$$\mathbf{F}_2^{(sym)}(\mathbf{q}_i, \mathbf{q}_j) = \Big[\mathbf{F}_2(\mathbf{q}_i, \mathbf{q}_j) + \mathbf{F}_2(\mathbf{q}_j, \mathbf{q}_i)\Big], \tag{7}$$

$$\begin{aligned}\mathbf{F}_3^{(sym)}(\mathbf{q}_i, \mathbf{q}_j, \mathbf{q}_\ell) = \Big[&\mathbf{F}_3(\mathbf{q}_i, \mathbf{q}_j, \mathbf{q}_\ell) + \mathbf{F}_3(\mathbf{q}_i, \mathbf{q}_\ell, \mathbf{q}_j) \\ &+ \mathbf{F}_3(\mathbf{q}_j, \mathbf{q}_i, \mathbf{q}_\ell) + \mathbf{F}_3(\mathbf{q}_\ell, \mathbf{q}_i, \mathbf{q}_j) \\ &+ \mathbf{F}_3(\mathbf{q}_j, \mathbf{q}_\ell, \mathbf{q}_i) + \mathbf{F}_3(\mathbf{q}_\ell, \mathbf{q}_j, \mathbf{q}_i)\Big]\end{aligned} \tag{8a}$$

With the aim of a simpler description of Fourier–Galerkin formalism, please note that dyadic interactions (interactions between two modes) are also possible whenever the tryadic nonlinear term $\mathbf{F}_3^{(sym)}$ contains the mean flow and other two harmonics, introduced in Section 3. So, in general dyadic interactions arise in the nonlinear term,

$$\mathbf{F}_2^{(dya)}(\mathbf{q}_i, \mathbf{q}_j) = \mathbf{F}_2^{(sym)}(\mathbf{q}_i, \mathbf{q}_j) + \mathbf{F}_3^{(sym)}(\mathbf{q}_i, \mathbf{q}_j, \mathbf{q}_0). \tag{9}$$

2.2. Linear stability

Before presenting the methodology used to compute a periodic cycle in the nonlinear regime, we recall the principle of Linear Stability Analysis (LSA) [20], which is the favored tool to detect the onset of such cycles from a previous steady state. Accordingly, LSA will be used in Section 5.1.1 to detect the critical Reynolds numbers associated with unsteadiness. Presentation of the LSA formalism also allows to introduce some notations which are used in the sequel.

The linear stability of compressible flows can be studied with a classical normal-mode analysis: the velocity and pressure fields are decomposed into a time-independent base flow, i.e. a steady-state, $\mathbf{q}_0 = [\rho, \mathbf{u}_0, T_0, p_0]$, and a generic three-dimensional small disturbance $\mathbf{q}' = \big[\rho', \mathbf{u}', T', p'\big]$. After introducing this decomposition into Eq. (3) and linearizing, it is found that the base flow is governed by the steady version of the Navier–Stokes equations, whereas the perturbation field is described by the linearized unsteady Navier–Stokes equations (LNSE) written as follows:

$$\mathbf{M}_{|\mathbf{q}_0}\frac{\partial \mathbf{q}'}{\partial t} + \mathbf{L}\mathbf{q}' + \mathbf{F}_2^{(sym)}(\mathbf{q}_0, \mathbf{q}') + \frac{1}{2}\mathbf{F}_3^{(sym)}(\mathbf{q}_0, \mathbf{q}_0, \mathbf{q}') = \mathbf{0}, \tag{10}$$

where $\mathbf{M}_{|\mathbf{q}_0} = \mathrm{diag}(1, \rho_0\mathbf{I}, \rho_0, 0)$ denotes the mass matrix evaluated at the steady state.

Global modes are modal non-trivial solutions of Eq. (10), which are expressed as follows:

$$\mathbf{q}' = \hat{\mathbf{q}}_\ell \; e^{\lambda_\ell t} + \text{c.c.}, \tag{11}$$

where λ_ℓ corresponds to the complex eigenvalue $(\sigma_\ell + \mathbf{i}\omega_\ell)$ and c.c. stands for complex conjugate and $\hat{\mathbf{q}}_\ell$ is the associated eigenmode. The real part of λ_ℓ represents the growth rate of the perturbation and the imaginary part ω_ℓ its circular frequency. For $\sigma_\ell > 0$, the flow is unstable whereas for $\sigma_\ell < 0$ it is stable. Introducing the ansatz Eq. (11) in the LNSE Eq. (10), we obtain the following generalized eigenvalue problem:

$$\mathbf{0} = \lambda_\ell \mathbf{M}_{|\mathbf{q}_0}\hat{\mathbf{q}}_\ell + L\mathcal{NS}_{|\mathbf{q}_0}(\hat{\mathbf{q}}_\ell) \tag{12}$$

with

$$\begin{aligned}L\mathcal{NS}_{|\mathbf{q}_0}(\hat{\mathbf{q}}_\ell) \equiv \;& \mathbf{L}\hat{\mathbf{q}}_\ell + \mathbf{F}_2^{(sym)}(\mathbf{q}_0, \hat{\mathbf{q}}_\ell) \\ +\; & \mathbf{F}_3^{(sym)}(\mathbf{q}_0, \mathbf{q}_0, \hat{\mathbf{q}}_\ell)\end{aligned} \tag{13}$$

3. Fourier–Galerkin method for Navier–Stokes equations

3.1. Fourier–Galerkin residual equation

Fourier–Galerkin method employs a truncated Fourier basis $\mathcal{F}_{\mathcal{N}}$, which is inherently periodic, thus perfectly suitable for the reconstruction of the periodic flow state:

$$\begin{aligned} \pi_N(\mathbf{q}) \equiv\ & \check{\mathbf{q}}_{(0)} + \sum_{n=1}^{N} \left[\check{\mathbf{q}}_{((n,c))} \cos(n\omega t) + \check{\mathbf{q}}_{((n,s))} \sin(n\omega t)\right] \\ \equiv\ & \check{\mathbf{Q}}^T \boldsymbol{\mathcal{F}}_{\boldsymbol{\mathcal{N}}} \\ \text{with } \boldsymbol{\mathcal{F}}_{\boldsymbol{\mathcal{N}}} =\ & \left[1, \cos(\omega t), \sin(\omega t), \ldots, \cos(N\omega t), \sin(N\omega t)\right]^T \\ \text{and } \check{\mathbf{Q}} =\ & \left[\check{\mathbf{q}}_{(0)}, \check{\mathbf{q}}_{((1,c))}, \check{\mathbf{q}}_{((1,s))}, \ldots, \check{\mathbf{q}}_{((N,c))}, \check{\mathbf{q}}_{((N,s))}\right]^T, \end{aligned} \tag{14}$$

where π_N is the projector operator onto the Fourier basis $\mathcal{F}_{\mathcal{N}}$; $\check{\mathbf{q}}_{((n,c))}(\mathbf{x})$ and $\check{\mathbf{q}}_{((n,s))}(\mathbf{x})$ are the coefficients of the Fourier series, in other words, they are two real nth-order harmonics describing the nonlinear perturbation at two instants separated by a quarter-period of oscillation. The projection π_N onto a finite Fourier basis $\mathcal{F}_{\mathcal{N}}$ introduces an error, nonetheless for smooth functions ($C^{\infty}(0, T)$) such an error decreases with an exponential rate, i.e. $\propto e^{-CN}, \quad C > 0$ with the number of harmonics N retained in the basis [21, Lemma 2.2].

The first step to obtain Fourier–Galerkin equations consists on the injection of the ansatz (14) into the unsteady Navier–Stokes equations (3). A Galerkin procedure is thus employed, i.e. the previously obtained equation is weighted with each term of the Fourier basis and then integrated over a period. Such a process is summarized below:

$$\mathcal{NS}(\mathbf{q}) \xrightarrow[\text{projection}]{\text{Fourier}} \mathcal{NS}(\pi_N(\mathbf{q})) \xrightarrow[\text{residual}]{\text{Weighted}} \begin{cases} \check{\mathbf{r}}^{(0)} = \dfrac{1}{T}\displaystyle\int_0^T \mathcal{NS}(\pi_N(\mathbf{q}))\mathrm{dt} \\ \check{\mathbf{r}}^{(n,c)} = \dfrac{2}{T}\displaystyle\int_0^T \mathcal{NS}(\pi_N(\mathbf{q}))\cos(n\omega t)\ \mathrm{dt} \\ \check{\mathbf{r}}^{(n,s)} = \dfrac{2}{T}\displaystyle\int_0^T \mathcal{NS}(\pi_N(\mathbf{q}))\sin(n\omega t)\ \mathrm{dt} \end{cases}$$

Finally, the residual vector $\check{\mathbf{R}} = \left[\check{\mathbf{r}}^{(0)}, \check{\mathbf{r}}^{(1,c)}, \check{\mathbf{r}}^{(1,s)}, \ldots, \check{\mathbf{r}}^{(N,c)}, \check{\mathbf{r}}^{(N,c)}\right]^T$ is equated to zero, i.e. $\check{\mathbf{R}} = \mathbf{0}$. In particular, the Fourier–Galerkin residual of the compressible Navier–Stokes equations written in primitive variables is expressed in compact operator notation as follows:

$$\check{\mathbf{r}}^{(0)} = L\mathcal{NS}_{|\check{\mathbf{q}}_{(0)}}\left(\check{\mathbf{q}}_{(0)}\right) + \check{\mathbf{F}}_2^{(0)}\left(\check{\mathbf{Q}}\right) + \check{\mathbf{F}}_3^{(0)}\left(\check{\mathbf{Q}}\right) \tag{15a}$$

$$\check{\mathbf{r}}^{(k,c)} = k\omega\mathbf{M}_{|\mathbf{q}_0}\check{\mathbf{q}}_{(k,s)} + L\mathcal{NS}_{|\check{\mathbf{q}}_{(0)}}\left(\check{\mathbf{q}}_{(k,c)}\right) + \check{\mathbf{F}}_2^{(k,c)}\left(\check{\mathbf{Q}}\right) + \check{\mathbf{F}}_3^{(k,c)}\left(\check{\mathbf{Q}}\right) \tag{15b}$$

$$\check{\mathbf{r}}^{(k,s)} = -k\omega\mathbf{M}_{|\mathbf{q}_0}\check{\mathbf{q}}_{(k,c)} + L\mathcal{NS}_{|\check{\mathbf{q}}_{(0)}}\left(\check{\mathbf{q}}_{(k,s)}\right) + \check{\mathbf{F}}_2^{(k,s)}\left(\check{\mathbf{Q}}\right) + \check{\mathbf{F}}_3^{(k,s)}\left(\check{\mathbf{Q}}\right) \tag{15c}$$

Linear terms contained in the operator $L\mathcal{NS}$ uniquely consist of interactions among harmonics of the same order and the mean flow. Dyadic and triadic interactions among harmonics are encoded in the nonlinear operators $\check{\mathbf{F}}_2^{(k)}$ and $\check{\mathbf{F}}_3^{(k)}$. For instance, $\check{\mathbf{F}}_2^{(0)}$ and $\check{\mathbf{F}}_3^{(0)}$, are the feedback terms among harmonic interactions and the mean flow. Similarly $\check{\mathbf{F}}_2^{(k,c)}$ and $\check{\mathbf{F}}_3^{(k,c)}$ (resp. $\check{\mathbf{F}}_2^{(k,s)}$ and $\check{\mathbf{F}}_3^{(k,s)}$) are the forcing terms of the kth cosine (resp. sinus) harmonic component. Interactions among different harmonics greatly increase with the degree of non linearity of the nonlinear operator. A detailed description of nonlinear terms may be found in Appendix. Eq. (15a) corresponds to the evolution of the mean flow component $\check{\mathbf{q}}_{(0)}$.

In addition to the $2N+1$ unknown fields constituting the Fourier expansion, the problem admits one extra scalar unknown, namely the frequency ω. The determination of the frequency it is equivalent to the determination of the period $T = \frac{2\pi}{\omega}$, which is measured as the distance in time between two solution points satisfying $\pi_N(\mathbf{q})(t+T) = \pi_N(\mathbf{q})(t)$. In addition, the problem is autonomous, which implies that for every phase shift ξ, $\pi_N(\mathbf{q})(t+\xi)$ is a solution of the system whenever $\pi_N(\mathbf{q})(t)$ is a solution. Therefore one can start measuring the period T at any solution point $\mathbf{q}(t+\xi)$ along the periodic orbit; in other words, the *phase-condition* that fixes the phase-shift ξ, it is an implicit equation of ω that serves to determine the unknown frequency. Any condition of the form $g(\check{\mathbf{Q}}) = 0$ where g is a linear function of the unknown fields can be used for this purpose. In practice, one can define the function g so as to coincide with a physically relevant integral quantity of the oscillating field at instant $t = 0$. For instance, for wake instability problems (Section 5.1.1) one can use the lift force exerted on the body, or for

oscillating jet problems (Section 5.2), one can use the oscillating flow rate across the aperture. At this stage we keep $g(\check{\mathbf{Q}}) = 0$ as an arbitrary linear function of the oscillating part of the flow. This function can always be decomposed formally as follows:

$$g(\check{\mathbf{Q}}) = \sum_{n=1}^{N} \left[g_{(n,c)}(\check{\mathbf{q}}_{(n,c)}) + g_{(n,s)}(\check{\mathbf{q}}_{(n,s)}) \right], \tag{16}$$

where $g_{(n,c)}$, $g_{(n,s)}$ are scalar-valued linear functions of the Fourier components.

3.2. Newton iteration method

Newton iteration is the chosen approach to solve the nonlinear Fourier–Galerkin system. At each step of the procedure, starting from an estimate $\left[\check{\mathbf{Q}}_n, \omega_n\right]^T$ of the solution, we look for an improved estimate defined as:

$$\check{\mathbf{Q}}_{n+1} = \check{\mathbf{Q}}_n + \delta\check{\mathbf{Q}}, \qquad \omega_{n+1} = \omega_n + \delta\omega. \tag{17}$$

Introducing Eq. (17) into the governing equations and linearizing with respect to perturbations $[\delta\check{\mathbf{Q}}, \delta\omega]$ leads to a linear system which has to be solved at each step of the procedure:

$$D\check{\mathbf{R}} \left[\delta\check{\mathbf{Q}}, \delta\omega\right]^T = -\left[\check{\mathbf{R}}(\check{\mathbf{Q}}_n), g(\check{\mathbf{Q}}_n)\right]^T, \tag{18a}$$

here $D\check{\mathbf{R}}$ denotes the Jacobian operator, written in block–matrix form as follows:

$$D\check{\mathbf{R}} = \begin{pmatrix} D\check{\mathbf{r}}^{(0;0)} & \cdots & D\check{\mathbf{r}}^{(0;k,c)} & D\check{\mathbf{r}}^{(0;k,s)} & \cdots & D_\omega\check{\mathbf{r}}^{(0)} \\ \vdots & \ddots & \vdots & \vdots & \ddots & \ddots \\ D\check{\mathbf{r}}^{(k,c;0)} & \cdots & D\check{\mathbf{r}}^{(k,c;k,c)} & D\check{\mathbf{r}}^{(k,c;k,s)} & \cdots & D_\omega\check{\mathbf{r}}^{(k,c)} \\ D\check{\mathbf{r}}^{(k,s;0)} & \cdots & D\check{\mathbf{r}}^{(k,s;k,c)} & D\check{\mathbf{r}}^{(k,s;k,s)} & \cdots & D_\omega\check{\mathbf{r}}^{(k,s)} \\ \vdots & \cdots & \vdots & \vdots & \ddots & \ddots \\ 0 & \cdots & g_{(k,c)} & g_{(k,s)} & \cdots & 0 \end{pmatrix} \tag{19}$$

and $D\check{\mathbf{r}}^{(k,c;j,s)}$ denotes the derivative of the residual term $\check{\mathbf{r}}^{(k,c)}$ with respect to the sinus component of the jth harmonic. Those block operators are defined as follows:

$$\begin{aligned} D\check{\mathbf{r}}^{(0)}\delta\check{\mathbf{Q}} &= L\mathcal{NS}_{|\check{\mathbf{q}}_{(0)}}\left(\delta\check{\mathbf{q}}_{(0)}\right) \\ &\quad + \left[D\check{\mathbf{F}}^{(0)}_{2|\check{\mathbf{Q}}} + D\check{\mathbf{F}}^{(0)}_{3|\check{\mathbf{Q}}}\right]\delta\check{\mathbf{Q}} \qquad (20a) \\ D\check{\mathbf{r}}^{(k,c)}\delta\check{\mathbf{Q}} &= k\omega\mathbf{M}\big|_{\delta\check{\mathbf{q}}_{(0)}}\check{\mathbf{q}}_{(k,s)} + k\omega\mathbf{M}\big|_{\check{\mathbf{q}}_{(0)}}\delta\check{\mathbf{q}}_{(k,s)} + L\mathcal{NS}_{|\check{\mathbf{q}}_{(0)}}\left(\delta\check{\mathbf{q}}_{(k,c)}\right) \\ &\quad + \left[D\check{\mathbf{F}}^{(k,c)}_{2|\check{\mathbf{Q}}} + D\check{\mathbf{F}}^{(k,c)}_{3|\check{\mathbf{Q}}}\right]\delta\check{\mathbf{Q}} \qquad (20b) \\ D\check{\mathbf{r}}^{(k,s)}\delta\check{\mathbf{Q}} &= -k\omega\mathbf{M}\big|_{\delta\check{\mathbf{q}}_{(0)}}\check{\mathbf{q}}_{(k,c)} - k\omega\mathbf{M}\big|_{\check{\mathbf{q}}_{(0)}}\delta\check{\mathbf{q}}_{(k,c)} + L\mathcal{NS}_{|\check{\mathbf{q}}_{(0)}}\left(\delta\check{\mathbf{q}}_{(k,s)}\right) \\ &\quad + \left[D\check{\mathbf{F}}^{(k,s)}_{2|\check{\mathbf{Q}}} + D\check{\mathbf{F}}^{(k,s)}_{3|\check{\mathbf{Q}}}\right]\delta\check{\mathbf{Q}} \qquad (20c) \end{aligned}$$

$$D_\omega\check{\mathbf{r}}^{(0)}\delta\omega = D_\omega\check{\mathbf{F}}^{(0)}_{2|\check{\mathbf{Q}}}\delta\omega \tag{21a}$$

$$D_\omega\check{\mathbf{r}}^{(k,c)}\delta\omega = \delta\omega\left(k\mathbf{M}\big|_{\check{\mathbf{q}}_{(0)}}\check{\mathbf{q}}_{(k,s)}\right) + D_\omega\check{\mathbf{F}}^{(k,c)}_{2|\check{\mathbf{Q}}}\delta\omega \tag{21b}$$

$$D_\omega\check{\mathbf{r}}^{(k,s)}\delta\omega = \delta\omega\left(-k\mathbf{M}\big|_{\check{\mathbf{q}}_{(0)}}\check{\mathbf{q}}_{(k,c)}\right) + D_\omega\check{\mathbf{F}}^{(k,s)}_{2|\check{\mathbf{Q}}}\delta\omega. \tag{21c}$$

With these notations, the action of each of the linear operators defined in Eq. (20) may be understood as the action of a row vector:

$$D\check{\mathbf{r}}^{(k,c)} = \left[D\check{\mathbf{r}}^{(k,c;0)}, D\check{\mathbf{r}}^{(k,c;1,c)}, D\check{\mathbf{r}}^{(k,c;1,s)}, \ldots, D\check{\mathbf{r}}^{(k,c;N,c)}, D\check{\mathbf{r}}^{(k,c;N,s)}\right]$$

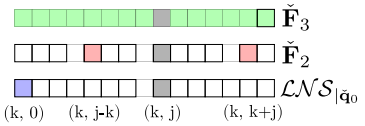

Fig. 1. Dependency pattern in the evaluation of the entry (k, j) in the derivative of each operator.

eventually leading to the block definition of the matrix defined in (19). Because the Fourier components with $k \neq 0$ involve both a cosine and a sine, a given entry (k, j) of the Jacobian operator $D\check{\mathbf{R}}$ is a 2×2 block if $k \neq 0$ and $j \neq 0$, a 2×1 block if $k \neq 0$ and $j = 0$, a 1×2 block if $k = 0$ and $j \neq 0$ or 1×1 block if $k = j = 0$. Each block is computed with respect to a set of harmonics and the mean component. The dependency pattern of each entry greatly depends on the nonlinearity of the operator: Fig. 1 schematizes the dependency stencil. Evaluation of the linear operator $L\mathcal{NS}_{|\check{\mathbf{q}}_{(0)}}$ depends uniquely on the mode k and on the mean component. Quadratic nonlinearities include interactions with modes $|k - j|$ and $j + k$. Whereas the evaluation of the nonlinear term $\check{\mathbf{F}}_3^{(k,s)}$ may depend on the full set of harmonics. For more details consider the detailed description provided in Appendix.

3.3. Resolution of the linear system of equations

The critical part in the algorithm is the resolution of the linear system (18a). Here, the GMRES method is used for the factorization of the full Jacobian $D\check{\mathbf{R}}$. Nonetheless, such an approach requires efficient preconditioning techniques to speed up convergence. In such a way the linear system Eq. (18a) is transformed into:

$$\mathbf{P}^{-1} D\check{\mathbf{R}} \left[\delta\check{\mathbf{Q}}_{n+1}, \delta\omega_{n+1}\right]^T = -\mathbf{P}^{-1} \left[\check{\mathbf{R}}(\check{\mathbf{Q}}_n), g(\check{\mathbf{Q}}_n, t = 0)\right]^T. \tag{22}$$

Three outer preconditioning techniques have been considered in this study: *Block Jacobi* and *Block Gauss Seidel* (upper and lower triangular). Let us detail these preconditioning techniques. In the following only the Fourier–Galerkin residual is considered. The line in the Jacobian operator that corresponds to the phase condition is included in the set of degrees of freedom of a $D\check{\mathbf{r}}^{(i)}$ block. In such a way the block composed of $D\check{\mathbf{r}}^{(i)}$ and the phase condition is not singular and the following preconditioning techniques are applicable.

Block-Jacobi preconditioning considers only blocks that are found on the diagonal, i.e. it does not take into account interactions with other Fourier components.

$$\mathbf{P}_{BJ}(\check{\mathbf{Q}}_n, \omega_n) = \begin{bmatrix} D\check{\mathbf{r}}^{(0)} & \dots & \mathbf{0} & \dots & \mathbf{0} \\ \vdots & \ddots & & & \vdots \\ \mathbf{0} & \dots & D\check{\mathbf{r}}^{(i)} & \dots & \mathbf{0} \\ \vdots & & & \ddots & \vdots \\ \mathbf{0} & \dots & \mathbf{0} & \dots & D\check{\mathbf{r}}^{(N)} \end{bmatrix} \tag{23}$$

Another possibility consists in the use of a Gauss–Seidel preconditioner. Upper triangular GS solves for each component by considering interactions with only higher harmonics.

$$\mathbf{P}_{GSU}(\check{\mathbf{Q}}_n, \omega_n) = \begin{bmatrix} D\check{\mathbf{r}}^{(0)} & \dots & D\check{\mathbf{r}}^{(0,i)} & \dots & D\check{\mathbf{r}}^{(0,N)} \\ \vdots & \ddots & & & \vdots \\ \mathbf{0} & \dots & D\check{\mathbf{r}}^{((i))} & \dots & D\check{\mathbf{r}}^{((i,N))} \\ \vdots & & & \ddots & \vdots \\ \mathbf{0} & \dots & \mathbf{0} & \dots & D\check{\mathbf{r}}^{(N)} \end{bmatrix} \tag{24}$$

Analogously, lower triangular block GS solves for every component by considering interactions uniquely with lower harmonics.

$$\mathbf{P}_{GSL}(\check{\mathbf{Q}}_n, \omega_n) = \begin{bmatrix} D\check{\mathbf{r}}^{(0)} & \dots & \mathbf{0} & \dots & \mathbf{0} \\ \vdots & \ddots & & & \vdots \\ D\check{\mathbf{r}}^{((i,0))} & \dots & D\check{\mathbf{r}}^{(i)} & \dots & \mathbf{0} \\ \vdots & & & \ddots & \vdots \\ D\check{\mathbf{r}}^{((N,0))} & \dots & D\check{\mathbf{r}}^{((N,i))} & \dots & D\check{\mathbf{r}}^{(N)} \end{bmatrix} \tag{25}$$

The preconditioned linear operator $\mathbf{P}^{-1} D\check{\mathbf{R}}$ of Eq. (22) in the case of BJ is composed of identity blocks in the diagonal and non-null blocks off-diagonal. Such a procedure is effective when the matrix is diagonally dominant, e.g. when harmonic components are of small amplitude. Let us consider the expression of $\mathbf{P}^{-1} D\check{\mathbf{R}}$, particularized for the above considered preconditioners:

$$\mathbf{P}_{BJ}^{-1} D\check{\mathbf{R}} = \mathbf{P}_{BJ}^{-1}\mathbf{P}_{GSL} + \mathbf{P}_{BJ}^{-1}\mathbf{P}_{GSU} - \mathbf{I} \tag{26a}$$

$$\mathbf{P}_{GSU}^{-1} D\check{\mathbf{R}} = \mathbf{P}_{GSU}^{-1}\mathbf{P}_{GSL} - \mathbf{P}_{GSU}^{-1} + \mathbf{I} \tag{26b}$$

$$\mathbf{P}_{GSL}^{-1} D\check{\mathbf{R}} = \mathbf{P}_{GSL}^{-1}\mathbf{P}_{GSU} - \mathbf{P}_{GSL}^{-1} + \mathbf{I}, \tag{26c}$$

in the above expressions the decomposition $D\check{\mathbf{R}} = [\mathbf{P}_{GSU} + \mathbf{P}_{GSL} - \mathbf{P}_{BJ}]$ is assumed. Preconditioners $\mathbf{P}$ require the factorization of diagonal blocks $D\check{\mathbf{r}}^{(i)}$. Two methods have been considered, exact factorization (LU) and Additive-Schwarz Method (ASM) with LU as sub-preconditioner.

3.4. Initial condition

When using a Newton method, an essential point for convergence is to start the process from an initial "guess" as close as possible to the expected solution. In parametric studies, continuation methods are commonly employed; namely, we select as initial condition a solution previously computed for close values of the parameters and repeat the procedure. The question remains on how to obtain a very first solution to initiate the continuation. One may start the process for parameter values just above the threshold for the onset of the cycle, where Linear Stability Analysis (LSA) gives a good clue of the solution. The simplest idea is to take the order-zero component as the mean flow of the LSA, namely $\check{\mathbf{Q}}_0 = \mathbf{q}_0$, set the order-one components to coincide with the linear eigenmode with some fitted amplitude ζ, namely $\check{\mathbf{Q}}_{1,c} = \zeta\, Re(\hat{\mathbf{q}})$, $\check{\mathbf{Q}}_{1,s} = -\zeta\, Im(\hat{\mathbf{q}})$, and initialize all higher-order components to zero. This method may need some fine hand-tuning of the amplitude ζ. A second, more elaborate method is to use *Weakly Nonlinear Analysis* (WNL), which provides an approximation of the solution close to the threshold up to order $N = 2$. This method is not detailed here; see [7] for a demonstration of this procedure in the incompressible case.

3.5. Summary

To summarize this section, a concise presentation of the whole procedure used to numerically solve the problem is given in algorithm 1.

4. Numerical approach

The `FreeFEM` software based on a finite element method is used to solve the problem numerically. An initial mesh is generated by decomposing the computational domain in triangles via a Delaunay–Voronoi algorithm. A variational formulation of the problem is then built using $\mathbb{P}_2$ (quadratic) elements for each component of the velocity and $\mathbb{P}_1$ (linear) elements for the pressure, temperature and density. Linear systems are solved with the `PETSc` library in a parallel context. The parallelization is carried out following a memory distributed paradigm. The system is decomposed in space into n_{cores} partitions, where n_{cores} is the number of cores. The $2N + 1$ Fourier components associated with the generic partition i are available for the processor i. Sponge regions are used to damp acoustic waves far from the domain of interest to prevent their reflection. The definition of the sponge region is the same as in Fani et al. [8].

Algorithm 1 Fourier-Galerkin for compressible Navier Stokes

Require: Initial guess $\left(\check{\mathbf{Q}}_0, \omega_0\right)$. Parameters M, Re.

function FOURIER-GALERKIN(M, Re, $\check{\mathbf{Q}}_0$, ω_0)
  n = 0
  while $|| \left[\check{\mathbf{R}}(\check{\mathbf{Q}}_n, \omega_n), g(\check{\mathbf{Q}}_n)\right]^T |_2 <$ tol **do**
    Evaluate $[\check{\mathbf{R}}(\check{\mathbf{Q}}_n, \omega_n), g(\check{\mathbf{Q}}_n)]$
    Evaluate $D\check{\mathbf{R}}(\check{\mathbf{Q}}_n, \omega_n)$ ▷ Full or matrix-vector function
    j = 0
    for $j < m$ **do**
      Assemble preconditioner $\mathbf{P}$ ▷ e.g. Block Jacobi
      $\mathbf{P}^{-1} D\check{\mathbf{R}}_{n,j} \left[\delta\check{\mathbf{Q}}_{n,j+1}, \delta\omega_{n,j+1}\right]^T = -\mathbf{P}^{-1}\check{\mathbf{R}}_{n,j}$ ▷ GMRES
      $(\check{\mathbf{Q}}_{n,j+1}, \omega_{n,j+1}) = (\check{\mathbf{Q}}_{n,j} + \delta\check{\mathbf{Q}}_{n,j+1}, \omega_{n,j} + \delta\omega_{n,j+1})$
      $j = j + 1$
    end for
    $(\check{\mathbf{Q}}_{n+1}, \omega_{n+1}) = (\check{\mathbf{Q}}_n + \delta\check{\mathbf{Q}}_{n+1}, \omega_n + \delta\omega_{n+1})$
    $n = n + 1$
  end while
  return $(\check{\mathbf{Q}}_{n+1}, \omega_{n+1})$
end function

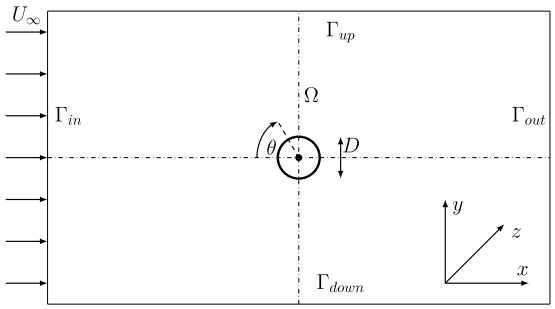

Fig. 2. Sketch of the computational domain Ω of the uniform flow past a circular cylinder.

Parametric studies and generation of figures are performed using Octave/Matlab with the aid of the generic drivers of the StabFem project (see a presentation of these functionalities in [7]). According to the philosophy of this project, a number of example codes generating sample results from the present paper are available online (https://gitlab.com/stabfem/StabFem).

Note that in the numerical implementation, we make an extensive use of mesh adaptation to ensure that spatial convergence is reached. The mesh is adapted either to a base flow and a linear eigenmode following the procedure explained in [7], or to the whole set of fields constituting the Fourier coefficients of the flow. Such adaptations are repeated several times during the parametric studies, and each time, the solution is projected onto the new mesh and used as starting point to relaunch the Newton iteration.

5. Results

5.1. Flow past a cylinder

5.1.1. Definition of the problem

The first example is the flow past a circular cylinder, a canonical configuration extensively studied in the literature in the incompressible [7,22] and compressible [8,23] setting. Cross-validations with literature are carried out to

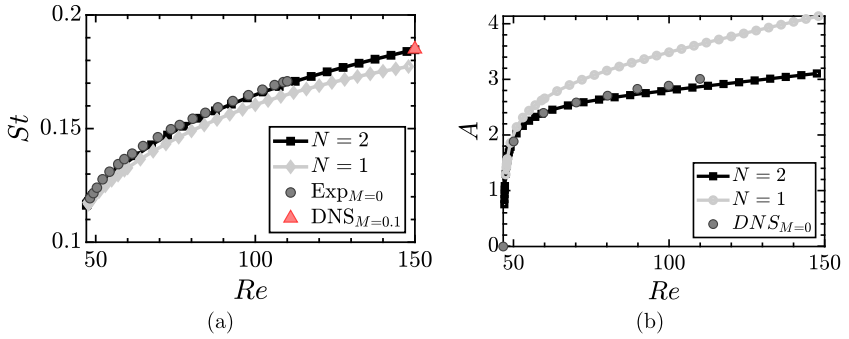

Fig. 3. (a) Evolution of the Strouhal fundamental frequency with Re. Experimental reference was taken from Carte et al. [24] and DNS data from Inoue et al. [25]. (b) Amplitude of the limit cycle. DNS reference data was reported by Mantic et al. [4].

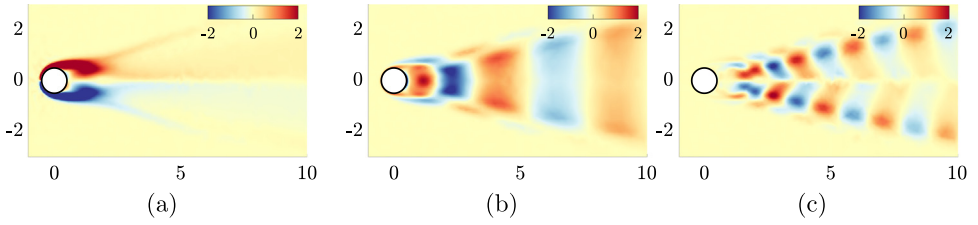

Fig. 4. Vorticity field at $Re = 150$ and $M = 10^{-1}$. (a) Mean component. (b) $\breve{\mathbf{q}}_{(1,c)}$ component. (c) $\breve{\mathbf{q}}_{(2,c)}$ component.

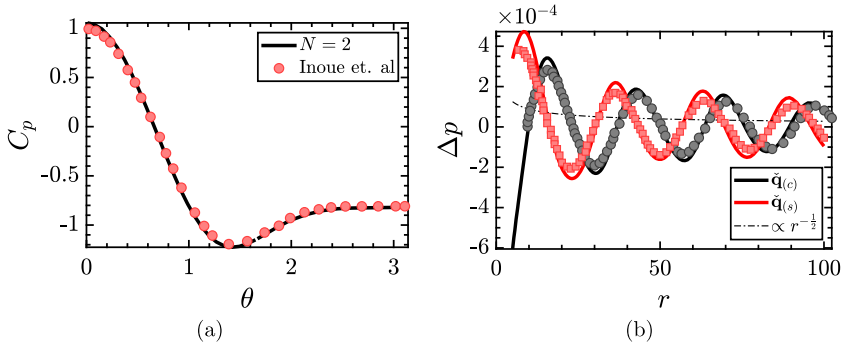

Fig. 5. $Re = 150$ and $M = 0.2$. (a) Pressure distribution around the cylinder. (b) Decay of pressure distribution at $\theta = \frac{\pi}{2}$. Markers report reference data from [25].

assess the precision of the method. In addition the numerical performance of linear solvers is evaluated in this case study.

A schematic representation of the computational domain Ω is shown in Fig. 2. Governing equations are complemented with the following boundary conditions: uniform velocity U_∞, density ρ_∞ and temperature T_∞ at boundaries Γ_{in}, Γ_{up}, Γ_{down}, Γ_{out} and no-slip adiabatic wall at the cylinder surface. The computational domain is a square of size $(300D \times 300D)$ which is immersed into a sponge domain of $(1000D \times 1000D)$. The chosen sponge size, which is around six wavelengths of the acoustic disturbance at $M = 10^{-2}$ in each direction, is sufficient to prevent any acoustic reflection from the boundaries of the domain Ω. The auxiliary function $g(\breve{\mathbf{Q}})$ needed to fix the phase of the cycle was defined as $g(\breve{\mathbf{Q}}) = F_y(t=0) \equiv \int_{\Gamma_w} \Big([-pI + \tau(\mathbf{u})]_{t=0} \cdot \mathbf{n} \Big) \cdot \mathbf{e}_y d\ell$, where Γ_w is the cylinder wall, so that the instant $t = 0$ corresponds to a zero of the oscillating lift exerted on the cylinder.

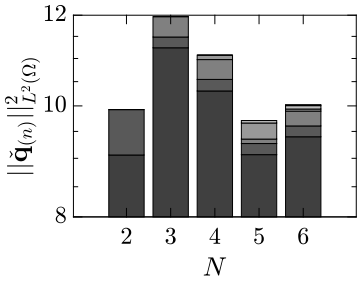

Fig. 6. Spectral reconstruction of the solution at $Re = 150$ and $M = 10^{-1}$. Gray-scale to distinguish the amplitude of each harmonic, lighter grays are used for higher harmonics.

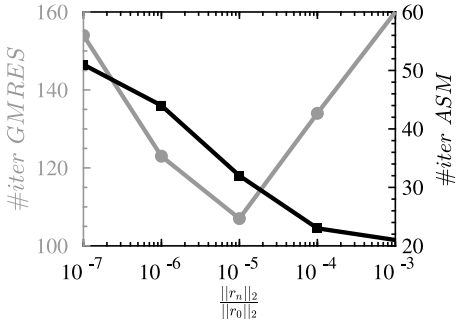

Fig. 7. Evolution of the total number of iterations of the inexact factorization with the ASM method of inner blocks with respect to the tolerance of the ASM procedure. Likewise, total number of GMRES iterations for the resolution of the nonlinear problem with respect to the ASM tolerance. Parameters $Re = 150$, $M = 0.1$, $N = 2$ with a numerical domain composed of $1.3 \cdot 10^5$ elements and the lower triangular Gauss Seidel as the outer preconditioner.

A comparison with other results reported in the literature is shown in Fig. 3. As can be seen (Fig. 3*a*), the frequency of the limit cycle is reliably evaluated even with a truncation to a single harmonic ($N = 1$). However, it fails to faithfully estimate its amplitude $A = \left(\sum_{n=1}^{N} \left\|\check{\mathbf{q}}_{(n)}\right\|^2_{L^2(\Omega)}\right)^{\frac{1}{2}}$. By contrast, a truncated Fourier basis with order $N = 2$ is sufficient to correctly predict the amplitude in the studied interval, namely $Re \in [Re_c, 100]$. For higher Reynolds numbers, e.g. $Re = 150$, a larger number of harmonics ($N > 2$) still modifies the spectral reconstruction, see Fig. 6. Such a figure displays the spectral content of the solution at $Re = 150$ and $M = 10^{-1}$. A high-fidelity reconstruction of the periodic solution can be obtained with $N \geq 4$, where the last mode displays a much smaller amplitude than the others.

Fig. 4 portrays the structure of the Fourier components reconstructing the vortex shedding cycle for $Re = 150$ and $M = 10^{-1}$. The structure of the mean flow and first harmonic are in good accordance with [8], but the second harmonic was not computed by these authors. Moreover, to assess the capability of the methodology to correctly reconstruct the solution both in the near field (governed by hydrodynamics) and in the far field (governed by acoustics), Fig. 5 represents the structure of the pressure field for the parameter values $M = 2 \cdot 10^{-1}$ and $Re = 150$, with a truncation $N = 2$. The comparison with reference data from the Direct Numerical Simulations (DNS) of Inoue et al. [25] is excellent, both for pressure along the cylinder wall (Fig. 5*a*), and along the vertical line defined by $x = 0$ (Fig. 5*b*).

5.1.2. Performance evaluation

Let us now use this test case to assess the performance of numerical algorithms to efficiently solve linear systems such as Eq. (18a). The tolerance to achieve the convergence of the Newton method corresponds to the L^2 norm of the Newton update of Eq. (18a), i.e. $\|\delta\mathbf{x}\|_{L^2} = \sqrt{\|\delta\check{\mathbf{Q}}\|^2_{L^2} + |\delta\omega|^2}$, lower than 10^{-8}. Likewise, the relative tolerance of the GMRES procedure (the ratio of the L^2 norm of the residual at the 1st iteration with respect to the ith iteration) for convergence is set to 10^{-5}. The resolution of the linear problems whose associated matrix is an inner

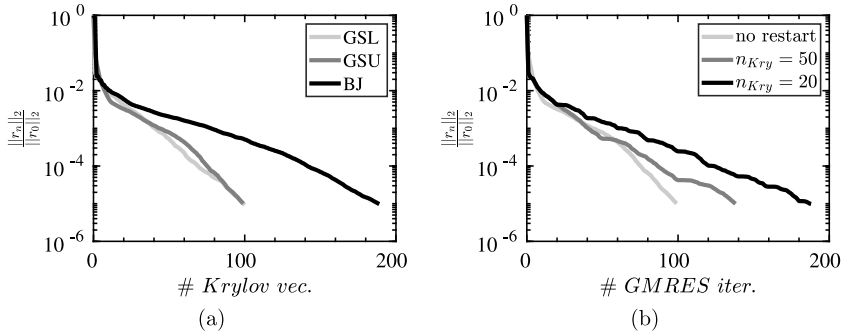

Fig. 8. Same parameters and mesh refinement as Fig. 7. (a) Evolution of relative residual versus cumulative Krylov vectors for the three preconditioners. (b) Evolution of the relative residual versus number of GMRES iterations for several restart configurations (outer preconditioner GSU).

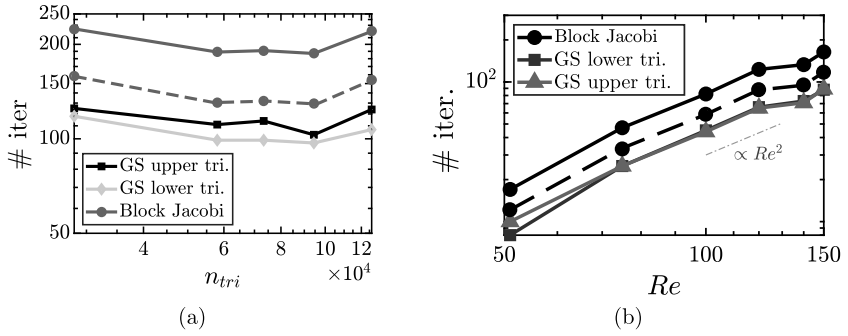

Fig. 9. (a) Dependency of GMRES iteration number with respect to the level of refinement of the computational domain at $Re = 150$ and $M = 0.1$ with $N = 2$. (b) Number of GMRES iterations as a function of Reynolds number and outer preconditioner with $N = 2$. Dashed line denotes the corrected number of GMRES iterations with the Block–Jacobi preconditioning.

block diagonal $D\check{\mathbf{r}}^{(i)}$, described in Section 3.3, is carried out with two approaches. If memory is not an issue, each block in the diagonal (of the Block-Jacobi or Gauss–Seidel preconditioners) is LU factorized. Otherwise an ASM preconditioner is used to solve the linear problems associated with inner blocks and the tolerance is varied from 10^{-3} to 10^{-7} (cf. Fig. 7). The GMRES approach takes 103 iterations with LU factorization of inner blocks; the number of GMRES iterations (107) reaches a minimum for a relative tolerance of the ASM approach of 10^{-5} (cf. Fig. 7), which shows weak independence of the GMRES procedure on the method used for the resolution of the inner diagonal blocks. On each GMRES iteration a Krylov vector is used (no restart). So the total number of Krylov vectors is equal to the number of GMRES iterations. Fig. 8a reports the evolution of the relative residual versus the cumulative number of Krylov vectors. In addition, on the same problem we tested the effect of n_{Kry}, the number of Krylov vectors retained in the basis (restarted GMRES). As expected the convergence rate deteriorates, but convergence is still reached in a reasonable number of iterations.

As reported in Fig. 9b, the number of GMRES iterations per Newton iteration increases quadratically with Reynolds number. In terms of GMRES iterations, the block diagonal preconditioning is less efficient than the other two but they follow the same trend as Re increases. Nonetheless, the GS preconditioning performs an additional number of $N(2N + 1)$ matrix–vector products, which is around 50% more block matrix–vector operations than BJ; therefore, one should correct the number of GMRES iterations by a factor 1.5, which is displayed in Fig. 9 with a dashed line. The methodology is also independent, as long as it is sufficient to reconstruct the solution from the number of harmonics and grid refinement, the latter reported in Fig. 9a. Finally a linear memory gain relative to an increasing length of the Fourier basis has been reported by Sierra et al. [26] with respect to the direct factorization of the full Jacobian operator.

Table 1
Wall-clock time required for convergence with eight processors for $Re = 150$ and numerical domain composed of $1.4 \cdot 10^4$ elements.

N/Method	Fourier–Galerkin	Explicit TSM	Implicit TSM
$M = 3 \cdot 10^{-1}$			
$N = 4$	2344 s	2451 s	8345 s
$N = 5$	2645 s	2992 s	9745 s
$N = 6$	3049 s	3250 s	11 121 s
$M = 10^{-1}$			
$N = 4$	2357 s	7745 s	22 355 s
$N = 5$	2591 s	8454 s	26 341 s
$N = 6$	3063 s	9721 s	31 545 s
$M = 10^{-2}$			
$N = 4$	2297 s	73 320 s	92 673 s
$N = 5$	2618 s	83 450 s	103 673 s
$N = 6$	3104 s	91 680 s	1 209 452 s

For the sake of comparison with other similar methodologies, authors have considered the Time spectral method (TSM), which solves the following nonlinear problem

$$\mathbf{M}^{\tau,K} \boldsymbol{D}_{FT} \check{\Omega}^{\tau,K} \boldsymbol{D}_{FT}^{-1} \mathbf{Q} + \mathbf{L}(\mathbf{Q}) + \mathbf{F}_2(\mathbf{Q},\mathbf{Q}) + \mathbf{F}_3(\mathbf{Q},\mathbf{Q},\mathbf{Q}) = \mathbf{0}, \tag{27}$$

where $\check{\Omega}_k^{\tau,K} = \begin{bmatrix} 0 & k\omega \\ -k\omega & 0 \end{bmatrix}$, $\check{\Omega}_0^{\tau,K} = 0$, $\mathbf{D}_{FT}$ denotes the discrete Fourier Transform operator (resp. $\mathbf{D}_{FT}^{-1}$ corresponds to the inverse Fourier transform operator) and $\mathbf{M}^{\tau,K}$ is the mass matrix $\mathbf{M}$ evaluated at each sampled instance. TSM requires the invertibility of forward and inverse discrete Fourier transforms. Therefore, the number of samples K must be fixed to $K = 2N+1$. TSM is commonly adapted from an already existing code via a *pseudo-time integration* approach (see e.g. [27]): an extra pseudo-time derivative $\mathbf{M}\frac{\partial \mathbf{Q}}{\partial t_{ps}}$ is added as a source term to Eq. (27). The resulting equations are solved in a pseudo-time direction until the stationary solution of the TSM formulation is reached. Note that the stationary solution of the TSM formulation is a spectral reconstruction of a periodic solution of the original system of equations. Such a technique is relative easy to implement as it only requires to add the TSM time-derivative on an already existing code. However, the pseudo-time marching approach is not able to directly compute an unstable periodic solution without stabilization procedures, see for instance BoostConv [28]. Furthermore, the efficiency of the approach depends on the CFL parameter of the pseudo-time step Δt_{ps} which is constrained as

$$\Delta t_{ps} = \frac{\mathrm{CFL}}{\frac{U_\infty}{h}(1+\frac{1}{M}) + \omega N} \tag{28}$$

where h is a measure of the size of the grid spacing and an extra term ωN is added due to the extra pseudo-time derivative. In acoustic applications, i.e. when $\frac{1}{M} \gg 1$ the CFL condition is roughly simplified to $\Delta t_{ps} \approx \frac{\mathrm{CFL}\ hM}{U_\infty}$; from a practical point of view, $O(\frac{1}{M})$ additional iterations are required with respect to the integration of the classical Navier–Stokes equations.

We carried out an accurate comparison at $Re = 150$ for three Mach numbers ($M = 3 \cdot 10^{-1}$, $M = 10^{-1}$ and $M = 10^{-2}$), with $N = 4, 5, 6$. The TSM data are computed by using the OpenSource SU2 code [29], where a finite volume implementation of the TSM method is available. The dual-time integration is realized with either the classical fourth-order Runge–Kutta method or with an implicit Euler iteration at the largest CFL allowed by stability constraints.

Regarding the initial condition, the Fourier–Galerkin–Newton–Krylov approach is initialized with a previous frequency reconstruction at another Mach or Reynolds number (either with the same or less number of harmonics N). Whereas, for the TSM, the initial solution consists of a snapshot of a DNS with the same set of parameters (Re, M). Such a choice was verified a posteriori to be faster than to initialize the TSM computation with a series of snapshots for another parameter configuration as it is done for FG. Additionally, TSM requires ω and T as an

Table 2
Average memory consumption for the resolution of the linear system Eq. (22) in a Newton iteration of the Fourier–Galerkin approach with $n_{cores} = 8$ with a numerical mesh of $7 \cdot 10^4$ elements for $Re = 150$, $M = 10^{-1}$.

	$N = 1$	$N = 2$	$N = 3$	$N = 4$	$N = 5$	$N = 6$
Mem.(Gb)	13.5 Gb	24.5 Gb	34.1 Gb	41.1 Gb	53.6 Gb	64.2 Gb

Table 3
Average memory consumption for the resolution of the linear system Eq. (22) in a Newton iteration of the Fourier–Galerkin approach with $N = 4$ and a mesh of $1.4 \cdot 10^5$ elements for $Re = 150$, $M = 10^{-1}$.

	$n_{cores} = 8$	$n_{cores} = 16$	$n_{cores} = 32$	$n_{cores} = 64$
Mem.(Gb)	75 Gb	93 Gb	129 Gb	171 Gb

input to evaluate the time derivative term. For our test, we have chosen a pair (ω, T) previously computed by a DNS. Sensitivity issues to an incorrect selection of the pair (ω, T) are discussed in Nimmagadda et al. [29]. Both approaches are computed with distinct codes and two different meshes has been used. In order to have a fair comparison, both numerical domains are composed of approximately $1.4 \cdot 10^4$ elements (triangles for FG and quads for TSM).

In reference to the numerical performance, let us first remark the similarity in terms of wall-clock time and memory requirements of the implicit integration of a dual time-step and a GMRES iteration of the Newton–Krylov–Fourier–Galerkin approach cf. [29,30]. However, a formal correspondence between explicit TSM and FG in terms of residual evaluations or matrix–vector products does not seem evident. Therefore, a numerical comparison of both approaches has been carried out in a eight cores Intel i7-9700 architecture. Table 1 reports the wall-clock time required for convergence (norm of the residual below 10^{-6}). Fourier–Galerkin and explicit TSM record a similar wall-clock time for $M = 3 \cdot 10^{-1}$, however TSM suffers a linear increase in the wall-clock time with the $\frac{1}{M}$ factor. Therefore, as the Mach number decreases FG rapidly outperforms TSM in wall-clock time due to the CFL constraint on the pseudo time.

Finally, let us discuss the memory requirements of the Newton–Krylov methodology on two meshes with two different levels of refinement. $\mathcal{M}_1$ is composed of around $1.4 \cdot 10^5$ elements and $\mathcal{M}_2$ has around $7 \cdot 10^4$ elements. Tests on memory requirements have been carried out on a cluster node equipped with 64 Intel(R) Xeon(R) CPU E5-4610 processors and 256 GB of RAM memory. The first test, carried out on mesh $\mathcal{M}_2$, assess the average memory consumption for the resolution of the linear system associated with each Newton iteration (Eq. (22)). These were performed with eighth processors for parameters $Re = 150$ and $M = 10^{-1}$ and upper Gauss–Seidel as preconditioning. Table 2 reports a sub-linear memory increasing with a empirical factor $N^{0.8}$. Such a factor is mainly due to the direct factorization of each block diagonal of the Jacobian Eq. (19). Similar results have been reported for the implicit TSM cf. [31,32]. The second performance test evaluates the memory scalability with respect to the number of processors; the results are reported in Table 3. A 30% increase of memory consumption is observed each time the number of processors is doubled. More studies regarding the scalability of the methodology have been previously carried out [26].

Finally, we highlight that the TSM wall-clock time reported in Table 1 requires the exact knowledge of the frequency ω. As a consequence, the total time required to get a given solution should take into account also the need to compute such a frequency. Our approach, on the other hand, directly characterizes the frequency within the global solution.

5.2. Whistling jet

The second test case is the flow passing through two circular holes in a plate (known as the hole-tone configuration). Such a flow configuration is encountered in many practical applications, including human whistling, wind instruments, whistling of a tea kettle [33], or birdcalls (devices used by hunters to imitate bird singing) [34,35].

In this study Fourier–Galerkin formalism is adopted with $N = 2, 3$ to study the self-sustained hydrodynamic instability and the radiation of sound past the unsteady onset. The physical domain and mesh structure are the same as in [35]. The numerical domain Ω is axisymmetric, as depicted in Fig. 10, with size $(800R_{h,1} \times 400R_{h,1})$ $(z \times r)$.

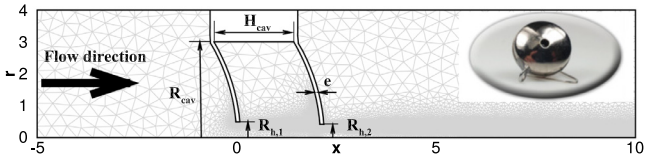

Fig. 10. Sketch of the hole-tone configuration, frame of reference and definition of geometrical parameters. An example of computational mesh is also reported in light gray. An actual birdcall is depicted in the upper right corner. For details about the used geometry see [35].

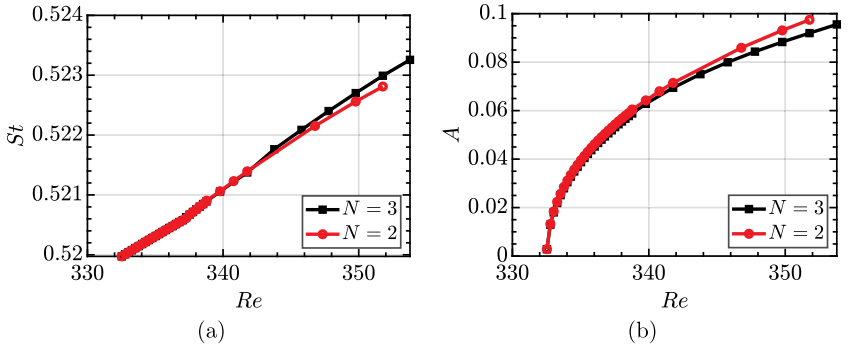

Fig. 11. (a) Evolution of the Strouhal fundamental frequency with Re. (b) Amplitude of the limit cycle.

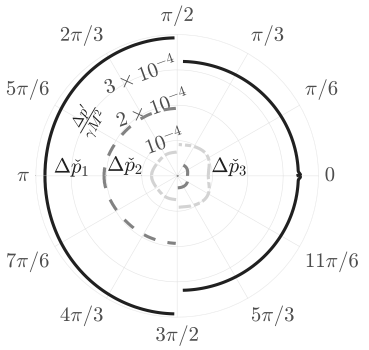

Fig. 12. Sound directivity at $Re = 350$ and $M = 0.02$ at a distance $r = 35$. Pressure variation $\Delta p'$ is scaled by γM^2.

The problem is complemented with appropriate boundary conditions: adiabatic no-slip walls, inlet mass flux such as the flow rate across the first hole is equal to unity and sponge layers of the order of three to four acoustic wavelengths at the far field. The sponge definition is the same as in [8]. The auxiliary function $g(\check{\mathbf{Q}})$ needed to fix the phase of the cycle was defined as $g(\check{\mathbf{Q}}) = \int_{\Gamma_{h1}} [(\mathbf{u}(t=0) - \mathbf{u}_0) \cdot \mathbf{n}]\, dS$, where Γ_{h1} is the cross section of the first hole, so that the instant $t = 0$ corresponds to a zero of the oscillating volume flow across the hole.

Fig. 11 shows the frequency and amplitude of the cycle as a function of Re, computed with respectively $N = 2$ and $N = 3$ truncations. In the current configuration, a truncated Fourier basis with order two seems sufficient since the results for $N = 2$ and $N = 3$ only differ by a few percents. Note that the flow is steady until the threshold of the first unsteadiness, which is located at $Re_c \approx 332.5$. This threshold value was first determined by linear stability analysis. The initial guess for the Fourier–Galerkin method with $Re > Re_c$ was obtained with a weakly nonlinear expansion and continuation was used afterwards while increasing Re.

The current approach provides direct access to the harmonic decomposition of sound directivity, reported in Fig. 12. The interaction between the jet and the two holes acts as a monopole aerodynamic source with different intensities upstream and downstream the cavity. The total sound radiation is of higher intensity upstream than downstream the obstacle, nonetheless the first harmonic behaves nearly as an isotropic monopole and the third harmonic radiates with higher intensity in the positive z direction.

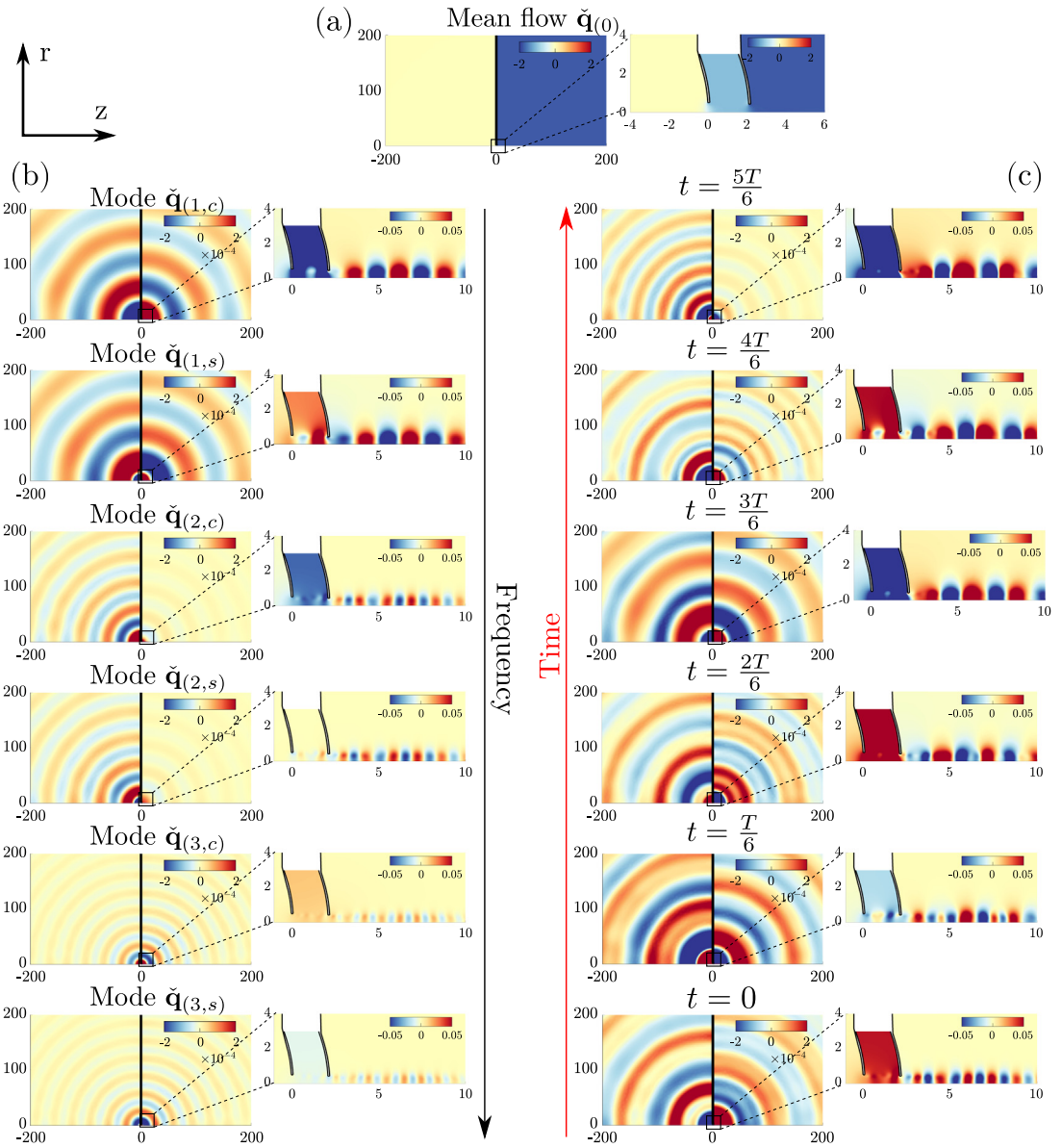

Fig. 13. Pressure component of acoustic and hydrodynamic perturbations at $Re = 350$ and $M = 0.02$ with $N = 3$. Pressure variation $\Delta p'$ is scaled by γM^2.

The whistling jet test case is a perfect example of what is called in the theory of numerical analysis a stiff problem. Namely, the ratio between the two velocity scales (acoustic and hydrodynamic) of the flow is large, therefore the time step is greatly constrained with respect to an application where the fast velocity scale is not of interest. A reconstruction of a time series of the periodic flow separating both hydrodynamic and acoustic scales is displayed in Fig. 13. Time integration with common numerical schemes, e.g. Runge–Kutta method, of a single point (fixed Re and M) of Fig. 11 requires the integration of several flow time scales, $T = \frac{1}{St}$. Moreover, the maximum time step of an explicit time integrator is governed by the fast time scale which is of the order $\Delta t \approx O(M)$. This implies that the simulation of the compressible Navier–Stokes equations at low-Mach-number would take approximately an $O(M^{-1})$ the amount of time necessary for a incompressible simulation. The analysis of acoustic radiation at

the low-Mach-number limit usually becomes prohibitively expensive and it requires the use of low-Mach-number limit approximations, where different scales are solved sequentially with a one-way feedback, see Nana et al. [36]. Fourier–Galerkin approach applied to compressible flows is intended to open new possibilities in the study of flows of acoustic and aeroacoustic interest at low-Mach-number since the CFL constraint does not hold. Additionally, the approach could be adapted to track quasiperiodic solutions by the consideration of two incommensurate frequencies and their interactions.

6. Conclusion

An efficient methodology for the computation of periodic flow solutions has been presented. The approach is based on the orthogonal projection of the sought solution on a truncated Fourier basis. The parametrized limit cycle is then directly accessible by solving a fixed point problem without the requirement of solving for transients. Krylov–Newton method has been selected for the resolution of the nonlinear residual problem Eq. (15). That sort of approach necessitates efficient preconditioning techniques, in the current study two layers of preconditioners are proposed and their performance has been tested in the flow past the circular cylinder in Section 5.1.1. Assembling of the Jacobian and residual operators, as well as the solution of the nonlinear problem is effectuated in a parallel framework. A comparison with similar spectral techniques has been demonstrated in Section 5.1.2, where it is shown the absence of a CFL-like condition for the Fourier–Galerkin approach. The latter property is significant for the reconstruction of solutions of stiff problems. Finally, the hole-tone configuration serves as a test case to demonstrate the ability of the technique to accurately reconstruct the two flow scales.

To conclude, we stress again that in addition to being efficient for computation of a cycle for a single set of parameters, our implementation is designed to perform parametric studies using a *continuation method*. Namely, once we have computed a cycle, taking it as an initial condition to relaunch the Newton iteration for nearby values of the parameter generally converges in only a few iterations. This procedure still needs an initial guess. In the present paper, the latter is constructed for parameters just above the instability onset using a weakly nonlinear expansion. Another possibility is to initialize the approach with a previous solution of a time-stepping simulation. This procedure has not been demonstrated here but might be simpler as any available software performing DNS may be used. Another advantage of the methodology is the ability to track unstable periodic cycles. Such solutions are not accessible with usual time-stepping DNS, but they are important when characterizing the dynamics from a dynamical system perspective, as their knowledge allows to understand more complex dynamics involving, for instance quasi-periodic orbits or chaotic attractors [37,38].

Declaration of competing interest

The authors declare that they have no known competing financial interests or personal relationships that could have appeared to influence the work reported in this paper.

Appendix. Fourier Galerkin equations

Let us detail the derivation of Fourier–Galerkin equations Eq. (15). For the sake of self-consistency let us first summarize the Fourier–Galerkin equations:

$$\check{\mathbf{r}}^{(0)} = L\mathcal{NS}_{|\check{\mathbf{q}}_{(0)}}\left(\check{\mathbf{q}}_{(0)}\right) + \check{\mathbf{F}}_2^{(0)}\left(\check{\mathbf{Q}}\right) + \check{\mathbf{F}}_3^{(0)}\left(\check{\mathbf{Q}}\right) \tag{A.1a}$$

$$\check{\mathbf{r}}^{(k,c)} = k\omega\mathbf{M}_{|\mathbf{q}_0}\check{\mathbf{q}}_{(k,s)} + L\mathcal{NS}_{|\check{\mathbf{q}}_{(0)}}\left(\check{\mathbf{q}}_{(k,c)}\right) + \check{\mathbf{F}}_2^{(k,c)}\left(\check{\mathbf{Q}}\right) + \check{\mathbf{F}}_3^{(k,c)}\left(\check{\mathbf{Q}}\right) \tag{A.1b}$$

$$\check{\mathbf{r}}^{(k,s)} = -k\omega\mathbf{M}_{|\mathbf{q}_0}\check{\mathbf{q}}_{(k,c)} + L\mathcal{NS}_{|\check{\mathbf{q}}_{(0)}}\left(\check{\mathbf{q}}_{(k,s)}\right) + \check{\mathbf{F}}_2^{(k,s)}\left(\check{\mathbf{Q}}\right) + \check{\mathbf{F}}_3^{(k,s)}\left(\check{\mathbf{Q}}\right) \tag{A.1c}$$

where nonlinear operators in the Fourier basis $\check{\mathbf{F}}^{(i)}\left(\check{\mathbf{Q}}\right)$ have been explicitly written using their quadratic and cubic contributions. The first step in an explicit derivation of Eq. (A.1) consists on the injection of the Fourier

Table A.4
Summary of trigonometric identities. c and s denote cosinus and sinus functions. Each term of the right (sum) is multiplied by a factor of $\frac{1}{4}$.

Product			Sum			
m	n	ℓ	$n+m+\ell$	$n+m-\ell$	$n+\ell-m$	$m+\ell-n$
c	c	c	c	c	c	c
c	c	s	s	$-s$	s	s
c	s	c	s	s	s	$-s$
c	s	s	$-c$	c	$-c$	c
s	c	c	s	s	$-s$	s
s	c	s	$-c$	c	c	$-c$
s	s	c	$-c$	$-c$	c	c
s	s	s	$-s$	s	s	s

representation of the sought solution Eq. (14) into the governing equations:

$$
\begin{aligned}
&\textstyle\sum_{n=1}^{N} L\mathcal{NS}_{|\check{\mathbf{q}}_{(0)}}\big(\check{\mathbf{q}}_{(0)}\big) + \Big[-k\omega\mathbf{M}_{|\mathbf{q}_0}\check{\mathbf{q}}_{(k,c)} + L\mathcal{NS}_{|\check{\mathbf{q}}_{(0)}}\big(\check{\mathbf{q}}_{(n,s)}\big)\Big]\sin(n\omega t)\\
&+\Big[k\omega\mathbf{M}_{|\mathbf{q}_0}\check{\mathbf{q}}_{(k,s)} + L\mathcal{NS}_{|\check{\mathbf{q}}_{(0)}}\big(\check{\mathbf{q}}_{(n,c)}\big)\Big]\cos(n\omega t)\\
&+\textstyle\sum_{n=1}^{N}\sum_{m=1}^{N}\Big[\,\mathbf{F}_2\big(\check{\mathbf{q}}_{(n,s)},\check{\mathbf{q}}_{(m,s)}\big)\sin(n\omega t)\sin(m\omega t)\\
&+\mathbf{F}_2\big(\check{\mathbf{q}}_{(n,s)},\check{\mathbf{q}}_{(m,c)}\big)\sin(n\omega t)\cos(m\omega t)\\
&+\mathbf{F}_2\big(\check{\mathbf{q}}_{(n,c)},\check{\mathbf{q}}_{(m,s)}\big)\cos(n\omega t)\sin(m\omega t)\\
&+\mathbf{F}_2\big(\check{\mathbf{q}}_{(n,c)},\check{\mathbf{q}}_{(m,c)}\big)\cos(n\omega t)\cos(m\omega t)\,\Big]\\
&+\textstyle\sum_{n=1}^{N}\sum_{m=1}^{N} n\omega\Big[\,-\mathbf{M}\big|_{\check{\mathbf{q}}_{(m,s)}}\check{\mathbf{q}}_{(n,c)}\sin(n\omega t)\sin(m\omega t)\\
&-\mathbf{M}\big|_{\check{\mathbf{q}}_{(m,c)}}\check{\mathbf{q}}_{(n,c)}\sin(n\omega t)\cos(m\omega t)\\
&+\mathbf{M}\big|_{\check{\mathbf{q}}_{(m,s)}}\check{\mathbf{q}}_{(n,s)}\cos(n\omega t)\sin(m\omega t)+\mathbf{M}\big|_{\check{\mathbf{q}}_{(m,c)}}\check{\mathbf{q}}_{(n,s)}\cos(n\omega t)\cos(m\omega t)\,\Big]\\
&+\textstyle\sum_{\ell=1}^{N}\sum_{n=1}^{N}\sum_{m=1}^{N}\Big[\,\mathbf{F}_3\big(\check{\mathbf{q}}_{(\ell,s)},\check{\mathbf{q}}_{(n,s)},\check{\mathbf{q}}_{(m,s)}\big)\sin(\ell\omega t)\sin(n\omega t)\sin(m\omega t)\\
&+\mathbf{F}_3\big(\check{\mathbf{q}}_{(\ell,c)},\check{\mathbf{q}}_{(n,s)},\check{\mathbf{q}}_{(m,s)}\big)\cos(\ell\omega t)\sin(n\omega t)\sin(m\omega t)\\
&+\mathbf{F}_3\big(\check{\mathbf{q}}_{(\ell,s)},\check{\mathbf{q}}_{(n,s)},\check{\mathbf{q}}_{(m,c)}\big)\sin(\ell\omega t)\sin(n\omega t)\cos(m\omega t)\\
&+\mathbf{F}_3\big(\check{\mathbf{q}}_{(\ell,c)},\check{\mathbf{q}}_{(n,s)},\check{\mathbf{q}}_{(m,c)}\big)\cos(\ell\omega t)\sin(n\omega t)\cos(m\omega t)\\
&+\mathbf{F}_3\big(\check{\mathbf{q}}_{(\ell,s)},\check{\mathbf{q}}_{(n,c)},\check{\mathbf{q}}_{(m,s)}\big)\sin(\ell\omega t)\cos(n\omega t)\sin(m\omega t)\\
&+\mathbf{F}_3\big(\check{\mathbf{q}}_{(\ell,c)},\check{\mathbf{q}}_{(n,c)},\check{\mathbf{q}}_{(m,s)}\big)\cos(\ell\omega t)\cos(n\omega t)\sin(m\omega t)\\
&+\mathbf{F}_3\big(\check{\mathbf{q}}_{(\ell,s)},\check{\mathbf{q}}_{(n,c)},\check{\mathbf{q}}_{(m,c)}\big)\sin(\ell\omega t)\cos(n\omega t)\cos(m\omega t)\\
&+\mathbf{F}_3\big(\check{\mathbf{q}}_{(\ell,c)},\check{\mathbf{q}}_{(n,c)},\check{\mathbf{q}}_{(m,c)}\big)\cos(\ell\omega t)\cos(n\omega t)\cos(m\omega t)\,\Big]=\mathbf{0}
\end{aligned}
\tag{A.2}
$$

Prior to the weighted residual step, it is convenient to work out trigonometric products of A.2 to $\cos(k\omega t)$ (resp. $\sin(k\omega t)$) where $0 \le k \le N$.

Table A.4 summarizes the set of identities to rearrange products of trigonometric terms into sum of terms of the Fourier basis. In the following, instead of working with non-symmetric operators as $\mathbf{F}_3$, let us use symmetric operators as $\mathbf{F}_3^{(sym)}$. Symmetric operators simplify the derivation of Fourier–Galerkin nonlinear terms $\check{\mathbf{F}}^{(i,c)}$ (resp. $\check{\mathbf{F}}^{(i,s)}$). Such a choice allows to uniquely consider a set of terms with argument $(n+m+\ell)\omega t$ and $(n+m-\ell)\omega t$ because the symmetric operator intrinsically considers the other set of terms whose arguments are $(n-m+\ell)\omega t$ and $(-n+m+\ell)\omega t$. Nonetheless, special care must be paid to consider unique terms, which is effectuated by the coefficient multiplying each term. In addition, the permutation of (m,n) by (n,m) does not change terms whose argument is $(n+m-\ell)\omega t$, which implies that only six terms of this kind are possible for each (m,n) $m+n \le N+k$, listed in Table A.5. Analogously, for terms whose arguments are of the kind $(n+m+\ell)\omega t$ only four terms are possible, reported in Table A.6 with their corresponding coefficients.

Table A.5
Coefficients of terms whose argument is of the kind $(n+m-\ell)\omega t$. Element pairs $(m,n)=(n,m)$ are considered the same.

Index (m,n)	ℓ	Coefficient $n+m-\ell=k$
(c,c)	c	$\frac{1}{8}c$
(c,s)	s	$\frac{1}{4}c$
(s,s)	c	$-\frac{1}{8}c$
(c,s)	c	$\frac{1}{4}s$
(c,c)	s	$-\frac{1}{8}s$
(s,s)	s	$\frac{1}{8}s$

Table A.6
Coefficients of terms whose argument is of the kind $(n+m+\ell)\omega t$. Same legend as in Table A.5.

Index (m,n,ℓ)	Coefficient $n+m+\ell=k$
(c,c,c)	$\frac{1}{24}c$
(c,s,s)	$-\frac{1}{8}c$
(c,c,s)	$\frac{1}{8}s$
(s,s,s)	$-\frac{1}{24}s$

A.1. Fourier–Galerkin nonlinear terms of third degree

Once the nonlinear terms of the third degree are written as coefficients of elements of the Fourier basis, the derivation of the Fourier–Galerkin expression of $\check{\mathbf{F}}_3^{(i)}(\check{\mathbf{Q}})$ is immediate:

$$\begin{aligned}\check{\mathbf{F}}_3^{(0)}(\check{\mathbf{Q}}) = \frac{1}{8}\sum_{\substack{m=1,n=1\\ m+n\le N}}^{N-1}\Big[&2\mathbf{F}_3^{(sym)}\big(\check{\mathbf{q}}_{(n,s)},\check{\mathbf{q}}_{(m,c)},\check{\mathbf{q}}_{(n+m,s)}\big)\\ &-\mathbf{F}_3^{(sym)}\big(\check{\mathbf{q}}_{(n,s)},\check{\mathbf{q}}_{(m,s)},\check{\mathbf{q}}_{(n+m,c)}\big)\\ &+\mathbf{F}_3^{(sym)}\big(\check{\mathbf{q}}_{(n,c)},\check{\mathbf{q}}_{(m,c)},\check{\mathbf{q}}_{(n+m,c)}\big)\Big]\end{aligned} \tag{A.3a}$$

$$\begin{aligned}\check{\mathbf{F}}_3^{(k,c)}(\check{\mathbf{Q}}) = \frac{1}{8}\sum_{\substack{m=1,n=1\\ m+n\le N+k}}^{N}\Big[&2\mathbf{F}_3^{(sym)}\big(\check{\mathbf{q}}_{(n,s)},\check{\mathbf{q}}_{(m,c)},\check{\mathbf{q}}_{(n+m-k,s)}\big)\\ &-\mathbf{F}_3^{(sym)}\big(\check{\mathbf{q}}_{(n,s)},\check{\mathbf{q}}_{(m,s)},\check{\mathbf{q}}_{(n+m-k,c)}\big)\\ &+\mathbf{F}_3^{(sym)}\big(\check{\mathbf{q}}_{(n,c)},\check{\mathbf{q}}_{(m,c)},\check{\mathbf{q}}_{(n+m-k,c)}\big)\Big]\\ +\frac{1}{24}\sum_{\substack{m=1,n=1\\ m+n\le k-1}}^{k-2}\Big[&\mathbf{F}_3^{(sym)}\big(\check{\mathbf{q}}_{(n,c)},\check{\mathbf{q}}_{(m,c)},\check{\mathbf{q}}_{(k-n-m,c)}\big)\\ &-3\mathbf{F}_3^{(sym)}\big(\check{\mathbf{q}}_{(n,c)},\check{\mathbf{q}}_{(m,s)},\check{\mathbf{q}}_{(k-n-m,s)}\big)\Big]\end{aligned} \tag{A.3b}$$

$$\begin{aligned}\check{\mathbf{F}}_3^{(k,s)}(\check{\mathbf{Q}}) = \frac{1}{8}\sum_{\substack{m=1,n=1\\ m+n\le N+k}}^{N}\Big[&2\mathbf{F}_3^{(sym)}\big(\check{\mathbf{q}}_{(n,c)},\check{\mathbf{q}}_{(m,s)},\check{\mathbf{q}}_{(n+m-k,c)}\big)\\ &-\mathbf{F}_3^{(sym)}\big(\check{\mathbf{q}}_{(n,c)},\check{\mathbf{q}}_{(m,c)},\check{\mathbf{q}}_{(n+m-k,s)}\big)\end{aligned}$$

$$+\ \mathbf{F}_3^{(sym)}\big(\check{\mathbf{q}}_{(n,s)},\check{\mathbf{q}}_{(m,s)},\check{\mathbf{q}}_{(n+m-k,s)}\big)\Big]$$
$$+\frac{1}{24}\sum_{\substack{m=1,n=1\\ m+n\leq k-1}}^{k-2}\Big[-\mathbf{F}_3^{(sym)}\big(\check{\mathbf{q}}_{(n,s)},\check{\mathbf{q}}_{(m,s)},\check{\mathbf{q}}_{(k-n-m,s)}\big)$$
$$+\ 3\mathbf{F}_3^{(sym)}\big(\check{\mathbf{q}}_{(n,c)},\check{\mathbf{q}}_{(m,c)},\check{\mathbf{q}}_{(k-n-m,s)}\big)\Big] \tag{A.3c}$$

A.2. Fourier-Galerkin nonlinear terms of second degree

Analogously, the quadratic operator $\check{\mathbf{F}}_2^{(i)}\big(\check{\mathbf{Q}}\big)$ is written as:

$$\check{\mathbf{F}}_2^{(0)}\big(\check{\mathbf{Q}}\big)=\frac{1}{4}\sum_{n=1}^{N}\Big[2\mathbf{F}^{\mathbf{M}}_{2,(n\omega,n\omega)}\big(\check{\mathbf{q}}_{(n,s)},\check{\mathbf{q}}_{(n,c)}\big)$$
$$+\ \mathbf{F}_2^{(dya)}\big(\check{\mathbf{q}}_{(n,c)},\check{\mathbf{q}}_{(n,c)}\big)$$
$$+\ \mathbf{F}_2^{(dya)}\big(\check{\mathbf{q}}_{(n,s)},\check{\mathbf{q}}_{(n,s)}\big)\Big] \tag{A.4a}$$

$$\check{\mathbf{F}}_2^{(k,c)}\big(\check{\mathbf{Q}}\big)=\frac{1}{2}\sum_{n=k+1}^{N}\Big[\mathbf{F}^{\mathbf{M}}_{2,((k-n)\omega,n\omega)}\big(\check{\mathbf{q}}_{(n,s)},\check{\mathbf{q}}_{(n-k,c)}\big)$$
$$+\ \mathbf{F}^{\mathbf{M}}_{2,(-n\omega,(n-k)\omega)}\big(\check{\mathbf{q}}_{(n-k,s)},\check{\mathbf{q}}_{(n,c)}\big)$$
$$+\ \mathbf{F}_2^{(dya)}\big(\check{\mathbf{q}}_{(n,c)},\check{\mathbf{q}}_{(n-k,c)}\big)$$
$$+\ \mathbf{F}_2^{(dya)}\big(\check{\mathbf{q}}_{(n,s)},\check{\mathbf{q}}_{(n-k,s)}\big)\Big]$$
$$+\frac{1}{4}\sum_{n=1}^{k-1}\Big[\mathbf{F}^{\mathbf{M}}_{2,(k\omega,k\omega)}\big(\check{\mathbf{q}}_{(n,s)},\check{\mathbf{q}}_{(k-n,c)}\big)$$
$$+\ \mathbf{F}_2^{(dya)}\big(\check{\mathbf{q}}_{(n,c)},\check{\mathbf{q}}_{(k-n,c)}\big)$$
$$-\ \mathbf{F}_2^{(dya)}\big(\check{\mathbf{q}}_{(n,s)},\check{\mathbf{q}}_{(k-n,s)}\big)\Big] \tag{A.4b}$$

$$\check{\mathbf{F}}_2^{(k,s)}\big(\check{\mathbf{Q}}\big)=\frac{1}{2}\sum_{n=k+1}^{N}\Big[\mathbf{F}^{\mathbf{M}}_{2,((n-k)\omega,-n\omega)}\big(\check{\mathbf{q}}_{(n,c)},\check{\mathbf{q}}_{(n-k,c)}\big)$$
$$+\ \mathbf{F}^{\mathbf{M}}_{2,(-n\omega,(n-k)\omega)}\big(\check{\mathbf{q}}_{(n-k,s)},\check{\mathbf{q}}_{(n,s)}\big)$$
$$+\ \mathbf{F}_2^{(dya)}\big(\check{\mathbf{q}}_{(n,s)},\check{\mathbf{q}}_{(n-k,c)}\big)$$
$$-\ \mathbf{F}_2^{(dya)}\big(\check{\mathbf{q}}_{(n,c)},\check{\mathbf{q}}_{(n-k,s)}\big)\Big]$$
$$+\frac{1}{4}\sum_{n=1}^{k-1}\Big[\mathbf{F}^{\mathbf{M}}_{2,((k-n)\omega,n\omega)}\big(\check{\mathbf{q}}_{(n,s)},\check{\mathbf{q}}_{(k-n,s)}\big)$$
$$+\ \mathbf{F}^{\mathbf{M}}_{2,(-n\omega,(n-k)\omega)}\big(\check{\mathbf{q}}_{(k-n,c)},\check{\mathbf{q}}_{(n,c)}\big)$$
$$+\ 2\mathbf{F}_2^{(dya)}\big(\check{\mathbf{q}}_{(k-n,c)},\check{\mathbf{q}}_{(n,s)}\big)\Big] \tag{A.4c}$$

Please also note the definition of the new dyadic operator $\mathbf{F}^{\mathbf{M}}_{2,(a,b)}$:

$$\mathbf{F}^{\mathbf{M}}_{2,(a,b)}\big(\hat{\mathbf{q}}_i,\hat{\mathbf{q}}_j\big)\equiv a\mathbf{M}\big|_{\hat{\mathbf{q}}_i}\hat{\mathbf{q}}_j+b\mathbf{M}\big|_{\hat{\mathbf{q}}_j}\hat{\mathbf{q}}_i \tag{A.5}$$

where $\mathbf{M}\big|_{\hat{\mathbf{q}}_j}=\mathrm{diag}(1,\hat{\rho}_j\mathbf{I},\hat{\rho}_j,0)$.

A.3. Jacobian operator

Let us consider the Jacobian operator of the Fourier–Galerkin residual Eq. (A.1):

$$D\check{\mathbf{r}}^{(0)}\delta\check{\mathbf{Q}} = L\mathcal{NS}_{|\check{\mathbf{q}}_{(0)}}\left(\delta\check{\mathbf{q}}_{(0)}\right) + \left[D\check{\mathbf{F}}^{(0)}_{2|\check{\mathbf{Q}}} + D\check{\mathbf{F}}^{(0)}_{3|\check{\mathbf{Q}}}\right]\delta\check{\mathbf{Q}} \tag{A.6a}$$

$$D\check{\mathbf{r}}^{(k,c)}\delta\check{\mathbf{Q}} = k\omega\mathbf{M}\big|_{\delta\check{\mathbf{q}}_{(0)}}\check{\mathbf{q}}_{(k,s)} + k\omega\mathbf{M}\big|_{\check{\mathbf{q}}_{(0)}}\delta\check{\mathbf{q}}_{(k,s)} + L\mathcal{NS}_{|\check{\mathbf{q}}_{(0)}}\left(\delta\check{\mathbf{q}}_{(k,c)}\right) + \left[D\check{\mathbf{F}}^{(k,c)}_{2|\check{\mathbf{Q}}} + D\check{\mathbf{F}}^{(k,c)}_{3|\check{\mathbf{Q}}}\right]\delta\check{\mathbf{Q}} \tag{A.6b}$$

$$D\check{\mathbf{r}}^{(k,s)}\delta\check{\mathbf{Q}} = -k\omega\mathbf{M}\big|_{\delta\check{\mathbf{q}}_{(0)}}\check{\mathbf{q}}_{(k,c)} - k\omega\mathbf{M}\big|_{\check{\mathbf{q}}_{(0)}}\delta\check{\mathbf{q}}_{(k,c)} + L\mathcal{NS}_{|\check{\mathbf{q}}_{(0)}}\left(\delta\check{\mathbf{q}}_{(k,s)}\right) + \left[D\check{\mathbf{F}}^{(k,s)}_{2|\check{\mathbf{Q}}} + D\check{\mathbf{F}}^{(k,s)}_{3|\check{\mathbf{Q}}}\right]\delta\check{\mathbf{Q}} \tag{A.6c}$$

where $L\mathcal{NS}^{(-k\omega)}_{|\check{\mathbf{q}}_{(0)}}\left(\check{\mathbf{q}}_{(k,c)}\right)$ and $\mathbf{M}\big|_{\delta\check{\mathbf{q}}_{(0)}}$ are linear operators. So, it is left to compute the derivative of nonlinear terms with respect to $\check{\mathbf{Q}}$, noted $D\check{\mathbf{F}}^{(k,s)}_{2|\check{\mathbf{Q}}}$ and $D\check{\mathbf{F}}^{(k,s)}_{3|\check{\mathbf{Q}}}$, along with the derivative with respect to ω:

$$D_\omega\check{\mathbf{r}}^{(0)}\delta\omega = D_\omega\check{\mathbf{F}}^{(0)}_{2|\check{\mathbf{Q}}}\delta\omega \tag{A.7a}$$

$$D_\omega\check{\mathbf{r}}^{(k,c)}\delta\omega = \delta\omega\left(k\mathbf{M}\big|_{\check{\mathbf{q}}_{(0)}}\check{\mathbf{q}}_{(k,s)}\right) + D_\omega\check{\mathbf{F}}^{(k,c)}_{2|\check{\mathbf{Q}}}\delta\omega \tag{A.7b}$$

$$D_\omega\check{\mathbf{r}}^{(k,s)}\delta\omega = \delta\omega\left(-k\mathbf{M}\big|_{\check{\mathbf{q}}_{(0)}}\check{\mathbf{q}}_{(k,c)}\right) + D_\omega\check{\mathbf{F}}^{(k,s)}_{2|\check{\mathbf{Q}}}\delta\omega \tag{A.7c}$$

Terms $D_\omega\check{\mathbf{F}}^{(0)}_{2|\check{\mathbf{Q}}}$, $D_\omega\check{\mathbf{F}}^{(k,s)}_{2|\check{\mathbf{Q}}}$ and $D_\omega\check{\mathbf{F}}^{(k,c)}_{2|\check{\mathbf{Q}}}$ will be detailed in the following section.

A.4. Jacobian operator of Fourier–Galerkin nonlinear terms of third degree

The Jacobian operator of Eq. (A.3) is a linear operator composed of 2×2 blocks for each harmonic component, except the mean flow component. Jacobian operators of high degree of nonlinearity lead to dense representations of derivative operators in the frequency domain, that is, the interactions between harmonics greatly depend on the degree of nonlinearity. The blocks of the Jacobian corresponding to the mean flow component are expressed as:

$$\begin{aligned} D\check{\mathbf{F}}^{(0;j,s)}_3\delta\check{\mathbf{q}}_{(j,s)} = {} & \frac{1}{4}\sum_{m=1}^{\min(N-j,1)}\mathbf{F}^{(sym)}_3\left(\delta\check{\mathbf{q}}_{(j,s)},\check{\mathbf{q}}_{(m,c)},\check{\mathbf{q}}_{(j+m,s)}\right) \\ & + \frac{1}{4}\sum_{m=1}^{\min(j-1,1)}\mathbf{F}^{(sym)}_3\left(\check{\mathbf{q}}_{(j-m,s)},\check{\mathbf{q}}_{(m,c)},\delta\check{\mathbf{q}}_{(j,s)}\right) \\ & - \frac{1}{4}\sum_{m=1}^{\min(N-j,1)}\mathbf{F}^{(sym)}_3\left(\delta\check{\mathbf{q}}_{(j,s)},\check{\mathbf{q}}_{(m,s)},\check{\mathbf{q}}_{(j+m,c)}\right) \end{aligned} \tag{A.8a}$$

$$\begin{aligned} D\check{\mathbf{F}}^{(0;j,c)}_3\delta\check{\mathbf{q}}_{(j,c)} = {} & \frac{1}{4}\sum_{m=1}^{\min(N-j,1)}\mathbf{F}^{(sym)}_3\left(\check{\mathbf{q}}_{(m,s)},\delta\check{\mathbf{q}}_{(j,c)},\check{\mathbf{q}}_{(j+m,s)}\right) \\ & - \frac{1}{8}\sum_{m=1}^{\min(j-1,1)}\mathbf{F}^{(sym)}_3\left(\check{\mathbf{q}}_{(j-m,s)},\check{\mathbf{q}}_{(m,s)},\delta\check{\mathbf{q}}_{(j,c)}\right) \\ & + \frac{1}{4}\sum_{m=1}^{\min(N-j,1)}\mathbf{F}^{(sym)}_3\left(\check{\mathbf{q}}_{(m,c)},\delta\check{\mathbf{q}}_{(j,c)},\check{\mathbf{q}}_{(j+m,c)}\right) \\ & + \frac{1}{8}\sum_{m=1}^{\min(j-1,1)}\mathbf{F}^{(sym)}_3\left(\check{\mathbf{q}}_{(j-m,c)},\check{\mathbf{q}}_{(m,c)},\delta\check{\mathbf{q}}_{(j,c)}\right) \end{aligned} \tag{A.8b}$$

Similarly, the cosinus lines of the Jacobian are expressed as:

$$
\begin{aligned}
D\check{\mathbf{F}}_3^{(k,c;j,s)}\delta\check{\mathbf{q}}_{(j,s)} = & \frac{1}{4}\sum_{m=\max(k-j+1,1)}^{\min(N+k-j,N)} \mathbf{F}_3^{(sym)}\left(\delta\check{\mathbf{q}}_{(j,s)}, \check{\mathbf{q}}_{(m,c)}, \check{\mathbf{q}}_{(j+m-k,s)}\right) \\
& + \frac{1}{4}\sum_{m=1}^{\min(j+k-1,N)} \mathbf{F}_3^{(sym)}\left(\check{\mathbf{q}}_{(j+k-m,s)}, \check{\mathbf{q}}_{(m,c)}, \delta\check{\mathbf{q}}_{(j,s)}\right) \\
& - \frac{1}{4}\sum_{m=\max(k-j+1,1)}^{\min(N+k-j,N)} \mathbf{F}_3^{(sym)}\left(\delta\check{\mathbf{q}}_{(j,s)}, \check{\mathbf{q}}_{(m,s)}, \check{\mathbf{q}}_{(j+m-k,c)}\right) \\
& - \frac{1}{4}\sum_{m=1}^{\min(k-j-1,1)} \mathbf{F}_3^{(sym)}\left(\delta\check{\mathbf{q}}_{(j,s)}, \check{\mathbf{q}}_{(m,c)}, \check{\mathbf{q}}_{(k-j-m,s)}\right)
\end{aligned} \tag{A.9a}
$$

$$
\begin{aligned}
D\check{\mathbf{F}}_3^{(k,c;j,c)}\delta\check{\mathbf{q}}_{(j,c)} = & \frac{1}{4}\sum_{m=\max(k-j+1,1)}^{\min(N+k-j,N)} \mathbf{F}_3^{(sym)}\left(\check{\mathbf{q}}_{(m,s)}, \delta\check{\mathbf{q}}_{(j,c)}, \check{\mathbf{q}}_{(j+m-k,s)}\right) \\
& - \frac{1}{8}\sum_{m=1}^{\min(j+k-1,N)} \mathbf{F}_3^{(sym)}\left(\check{\mathbf{q}}_{(m,s)}, \check{\mathbf{q}}_{(j+k-m,s)}, \delta\check{\mathbf{q}}_{(j,c)}\right) \\
& + \frac{1}{4}\sum_{m=\max(k-j+1,1)}^{\min(N+k-j,N)} \mathbf{F}_3^{(sym)}\left(\check{\mathbf{q}}_{(m,c)}, \delta\check{\mathbf{q}}_{(j,c)}, \check{\mathbf{q}}_{(j+m-k,c)}\right) \\
& + \frac{1}{8}\sum_{m=1}^{\min(j+k-1,N)} \mathbf{F}_3^{(sym)}\left(\check{\mathbf{q}}_{(m,c)}, \check{\mathbf{q}}_{(j+k-m,c)}, \delta\check{\mathbf{q}}_{(j,c)}\right) \\
& + \frac{1}{8}\sum_{m=1}^{\min(k-j-1,1)} \mathbf{F}_3^{(sym)}\left(\check{\mathbf{q}}_{(m,c)}, \check{\mathbf{q}}_{(k-m-j,c)}, \delta\check{\mathbf{q}}_{(j,c)}\right) \\
& - \frac{1}{8}\sum_{m=1}^{\min(k-j-1,1)} \mathbf{F}_3^{(sym)}\left(\delta\check{\mathbf{q}}_{(j,c)}, \check{\mathbf{q}}_{(m,s)}, \check{\mathbf{q}}_{(k-m-j,s)}\right)
\end{aligned} \tag{A.9b}
$$

and finally the derivative of sinus components:

$$
\begin{aligned}
D\check{\mathbf{F}}_3^{(k,s;j,s)}\delta\check{\mathbf{q}}_{(j,s)} = & \frac{1}{4}\sum_{m=\max(k-j+1,1)}^{\min(N+k-j,N)} \mathbf{F}_3^{(sym)}\left(\delta\check{\mathbf{q}}_{(j,s)}, \check{\mathbf{q}}_{(m,c)}, \check{\mathbf{q}}_{(j+m-k,c)}\right) \\
& - \frac{1}{8}\sum_{m=1}^{\min(j+k-1,N)} \mathbf{F}_3^{(sym)}\left(\check{\mathbf{q}}_{(j+k-m,c)}, \check{\mathbf{q}}_{(m,c)}, \delta\check{\mathbf{q}}_{(j,s)}\right) \\
& + \frac{1}{4}\sum_{m=\max(k-j+1,1)}^{\min(N+k-j,N)} \mathbf{F}_3^{(sym)}\left(\delta\check{\mathbf{q}}_{(j,s)}, \check{\mathbf{q}}_{(m,s)}, \check{\mathbf{q}}_{(j+m-k,s)}\right) \\
& + \frac{1}{8}\sum_{m=1}^{\min(j+k-1,N)} \mathbf{F}_3^{(sym)}\left(\check{\mathbf{q}}_{(j+k-m,s)}, \check{\mathbf{q}}_{(m,s)}, \delta\check{\mathbf{q}}_{(j,s)}\right) \\
& - \frac{1}{8}\sum_{m=1}^{\min(k-j-1,1)} \mathbf{F}_3^{(sym)}\left(\delta\check{\mathbf{q}}_{(j,s)}, \check{\mathbf{q}}_{(m,s)}, \check{\mathbf{q}}_{(k-j-m,s)}\right) \\
& + \frac{1}{8}\sum_{m=1}^{\min(k-j-1,1)} \mathbf{F}_3^{(sym)}\left(\check{\mathbf{q}}_{(k-j-m,c)}, \check{\mathbf{q}}_{(m,c)}, \delta\check{\mathbf{q}}_{(j,s)}\right)
\end{aligned} \tag{A.10a}
$$

$$
\begin{aligned}
D\check{\mathbf{F}}_3^{(k,s;j,c)}\delta\check{\mathbf{q}}_{(j,c)} = & \frac{1}{4}\sum_{m=\max(k-j+1,1)}^{\min(N+k-j,N)} \mathbf{F}_3^{(sym)}\big(\check{\mathbf{q}}_{(m,s)}, \delta\check{\mathbf{q}}_{(j,s)}, \check{\mathbf{q}}_{(j+m-k,s)}\big) \\
& + \frac{1}{4}\sum_{m=1}^{\min(j+k-1,N)} \mathbf{F}_3^{(sym)}\big(\check{\mathbf{q}}_{(m,c)}, \check{\mathbf{q}}_{(j+k-m,s)}, \delta\check{\mathbf{q}}_{(j,c)}\big) \\
& - \frac{1}{4}\sum_{m=\max(k-j+1,1)}^{\min(N+k-j,N)} \mathbf{F}_3^{(sym)}\big(\check{\mathbf{q}}_{(m,c)}, \delta\check{\mathbf{q}}_{(j,c)}, \check{\mathbf{q}}_{(j+m-k,s)}\big) \\
& + \frac{1}{4}\sum_{m=1}^{\min(k-j-1,1)} \mathbf{F}_3^{(sym)}\big(\delta\check{\mathbf{q}}_{(j,c)}, \check{\mathbf{q}}_{(m,c)}, \check{\mathbf{q}}_{(k-m-j,s)}\big)
\end{aligned} \tag{A.10b}
$$

A.5. Jacobian operator of Fourier–Galerkin nonlinear terms of second degree

Let us now detail the expressions of quadratic nonlinear terms. Please note that some of the terms do not appear because their index is higher than N or lower than one. In the following, those terms whose index is equal to $k-j$ may uniquely be present if $j \leq k+1$. Similarly those terms whose index is $k+j$ should respect $k+j \leq N$. Terms which do not satisfy the previous relations are implicitly suppressed.

$$
D\check{\mathbf{F}}^{(0)}\delta\check{\mathbf{q}}_{(j,c)} = \frac{1}{2}\mathbf{F}^{\mathbf{M}}_{2,(-j\omega,j\omega)}\big(\check{\mathbf{q}}_{(j,s)}, \delta\check{\mathbf{q}}_{(j,c)}\big) + \frac{1}{2}\mathbf{F}_2^{(dya)}\big(\check{\mathbf{q}}_{(j,c)}, \delta\check{\mathbf{q}}_{(j,c)}\big) \tag{A.11a}
$$

$$
D\check{\mathbf{F}}^{(0)}\delta\check{\mathbf{q}}_{(j,s)} = \frac{1}{2}\mathbf{F}^{\mathbf{M}}_{2,(-j\omega,j\omega)}\big(\delta\check{\mathbf{q}}_{(j,s)}, \check{\mathbf{q}}_{(j,c)}\big) + \frac{1}{2}\mathbf{F}_2^{(dya)}\big(\check{\mathbf{q}}_{(n,s)}, \delta\check{\mathbf{q}}_{(n,s)}\big) \tag{A.11b}
$$

$$
\begin{aligned}
D\check{\mathbf{F}}_2^{(k,c;j,s)}\delta\check{\mathbf{q}}_{(j,s)} = & \frac{1}{2}\Big[\mathbf{F}^{\mathbf{M}}_{2,((k-j)\omega,j\omega)}\big(\delta\check{\mathbf{q}}_{(j,s)}, \check{\mathbf{q}}_{(j-k,c)}\big) \\
& + \mathbf{F}^{\mathbf{M}}_{2,(-(j+k)\omega,j\omega)}\big(\delta\check{\mathbf{q}}_{(j,s)}, \check{\mathbf{q}}_{(j+k,c)}\big) \\
& + \mathbf{F}_2^{(dya)}\big(\delta\check{\mathbf{q}}_{(j,s)}, \check{\mathbf{q}}_{(j-k,s)}\big) + \mathbf{F}_2^{(dya)}\big(\check{\mathbf{q}}_{(j+k,s)}, \delta\check{\mathbf{q}}_{(j,s)}\big) \Big] \\
& + \frac{1}{4}\Big[\mathbf{F}^{\mathbf{M}}_{2,(k\omega,k\omega)}\big(\delta\check{\mathbf{q}}_{(j,s)}, \check{\mathbf{q}}_{(k-j,c)}\big) \\
& - 2\mathbf{F}_2^{(dya)}\big(\delta\check{\mathbf{q}}_{(j,s)}, \check{\mathbf{q}}_{(k-j,s)}\big) \Big]
\end{aligned} \tag{A.11c}
$$

$$
\begin{aligned}
D\check{\mathbf{F}}_2^{(k,c;j,c)}\delta\check{\mathbf{q}}_{(j,c)} = & \frac{1}{2}\Big[\mathbf{F}^{\mathbf{M}}_{2,((j+k)\omega,-j\omega)}\big(\delta\check{\mathbf{q}}_{(j,c)}, \check{\mathbf{q}}_{(j+k,s)}\big) \\
& + \mathbf{F}^{\mathbf{M}}_{2,((j-k)\omega,-j\omega)}\big(\delta\check{\mathbf{q}}_{(j,c)}, \check{\mathbf{q}}_{(j-k,s)}\big) \\
& + \mathbf{F}_2^{(dya)}\big(\check{\mathbf{q}}_{(j+k,c)}, \delta\check{\mathbf{q}}_{(j,c)}\big) + \mathbf{F}_2^{(dya)}\big(\delta\check{\mathbf{q}}_{(j,c)}, \check{\mathbf{q}}_{(j-k,c)}\big) \Big] \\
& + \frac{1}{4}\Big[\mathbf{F}^{\mathbf{M}}_{2,(k\omega,k\omega)}\big(\check{\mathbf{q}}_{(j,s)}, \delta\check{\mathbf{q}}_{(k-j,c)}\big) \\
& + 2\mathbf{F}_2^{(dya)}\big(\delta\check{\mathbf{q}}_{(j,c)}, \check{\mathbf{q}}_{(k-j,c)}\big) \Big]
\end{aligned} \tag{A.11d}
$$

$$
\begin{aligned}
D\check{\mathbf{F}}_2^{(k,s;j,c)}\delta\check{\mathbf{q}}_{(j,c)} = & \frac{1}{2}\Big[\mathbf{F}^{\mathbf{M}}_{2,(j\omega,-(j+k)\omega)}\big(\check{\mathbf{q}}_{(j+k,c)}, \delta\check{\mathbf{q}}_{(j,c)}\big) \\
& + \mathbf{F}^{\mathbf{M}}_{2,((j-k)\omega,-j\omega)}\big(\delta\check{\mathbf{q}}_{(j,c)}, \check{\mathbf{q}}_{(j-k,c)}\big) \\
& + \mathbf{F}_2^{(dya)}\big(\check{\mathbf{q}}_{(j+k,s)}, \delta\check{\mathbf{q}}_{(j,c)}\big) \\
& - \mathbf{F}_2^{(dya)}\big(\delta\check{\mathbf{q}}_{(j,c)}, \check{\mathbf{q}}_{(j-k,s)}\big) \\
& + \mathbf{F}^{\mathbf{M}}_{2,(-j\omega,(j-k)\omega)}\big(\check{\mathbf{q}}_{(j-k,c)}, \delta\check{\mathbf{q}}_{(j,c)}\big) \\
& + \mathbf{F}_2^{(dya)}\big(\delta\check{\mathbf{q}}_{(j,c)}, \check{\mathbf{q}}_{(j-k,s)}\big) \Big]
\end{aligned} \tag{A.11e}
$$

$$
D\check{\mathbf{F}}_2^{(k,s;j,s)}\delta\check{\mathbf{q}}_{(j,s)} = \frac{1}{2}\Big[\mathbf{F}^{\mathbf{M}}_{2,(-(j+k)\omega,j\omega)}\big(\delta\check{\mathbf{q}}_{(j,s)}, \check{\mathbf{q}}_{(j+k,s)}\big)
$$

$$+ \mathbf{F}^{\mathbf{M}}_{2,(-j\omega,(j-k)\omega)}\left(\check{\mathbf{q}}_{(j-k,s)}, \delta\check{\mathbf{q}}_{(j,s)}\right)$$
$$+ \mathbf{F}^{(dya)}_{2}\left(\delta\check{\mathbf{q}}_{(j,s)}, \check{\mathbf{q}}_{(j-k,c)}\right)$$
$$- \mathbf{F}^{(dya)}_{2}\left(\check{\mathbf{q}}_{(j+k,c)}, \delta\check{\mathbf{q}}_{(j,s)}\right)$$
$$+ \mathbf{F}^{\mathbf{M}}_{2,((k-j)\omega,j\omega)}\left(\delta\check{\mathbf{q}}_{(j,s)}, \check{\mathbf{q}}_{(k-j,s)}\right)$$
$$+ \mathbf{F}^{(dya)}_{2}\left(\check{\mathbf{q}}_{(k-j,c)}, \delta\check{\mathbf{q}}_{(j,s)}\right) \Big] \tag{A.11f}$$

Prior to the introduction of the derivative of the quadratic nonlinear term with respect to ω, let us define the derivative with respect to ω of the generic operator $\mathbf{F}^{\mathbf{M}}_{2,(j\omega,k\omega)}\left(\check{\mathbf{q}}_{(a)}, \check{\mathbf{q}}_{(b)}\right)$:

$$D_\omega \mathbf{F}^{\mathbf{M}}_{2,(j\omega,k\omega)}\left(\check{\mathbf{q}}_{(a)}, \check{\mathbf{q}}_{(b)}\right) = \left(j\mathbf{M}\big|_{\check{\mathbf{q}}_{(a)}}\check{\mathbf{q}}_{(b)} + k\mathbf{M}\big|_{\check{\mathbf{q}}_{(b)}}\check{\mathbf{q}}_{(a)}\right) \tag{A.12}$$

Then the definition of $D_\omega\check{\mathbf{F}}^{(0)}_{2|\check{\mathbf{Q}}}$, $D_\omega\check{\mathbf{F}}^{(k,s)}_{2|\check{\mathbf{Q}}}$ and $D_\omega\check{\mathbf{F}}^{(k,c)}_{2|\check{\mathbf{Q}}}$ is as follows,

$$D_\omega\check{\mathbf{F}}^{(0)}_{2|\check{\mathbf{Q}}}\delta\omega = \frac{1}{2}\delta\omega\sum_{j=1}^{N} D_\omega\mathbf{F}^{\mathbf{M}}_{2,(-j,j)}\left(\check{\mathbf{q}}_{(j,s)}, \check{\mathbf{q}}_{(j,c)}\right) \tag{A.13a}$$

$$D_\omega\check{\mathbf{F}}^{(k,c)}_{2|\check{\mathbf{Q}}}\delta\omega = \delta\omega\Bigg[\frac{1}{4}\sum_{j=1}^{k-1} D_\omega\mathbf{F}^{\mathbf{M}}_{2,(k,k)}\left(\check{\mathbf{q}}_{(j,c)}, \check{\mathbf{q}}_{(k-j,s)}\right)$$
$$+ \frac{1}{2}\sum_{j=i+1}^{N} D_\omega\mathbf{F}^{\mathbf{M}}_{2,(k-j,-j)}\left(\check{\mathbf{q}}_{(j,c)}, \check{\mathbf{q}}_{(k-j,s)}\right)$$
$$+ \frac{1}{2}\sum_{j=i+1}^{N} D_\omega\mathbf{F}^{\mathbf{M}}_{2,(k-j,j)}\left(\check{\mathbf{q}}_{(j,s)}, \check{\mathbf{q}}_{(k-j,c)}\right)\Bigg] \tag{A.13b}$$

$$D_\omega\check{\mathbf{F}}^{(k,s)}_{2|\check{\mathbf{Q}}}\delta\omega = \delta\omega\Bigg[\frac{1}{4}\sum_{j=1}^{k-1} D_\omega\mathbf{F}^{\mathbf{M}}_{2,(k-j,j)}\left(\check{\mathbf{q}}_{(j,s)}, \check{\mathbf{q}}_{(k-j,s)}\right)$$
$$+ \frac{1}{4}\sum_{j=1}^{k-1} D_\omega\mathbf{F}^{\mathbf{M}}_{2,(k-j,-j)}\left(\check{\mathbf{q}}_{(j,c)}, \check{\mathbf{q}}_{(k-j,c)}\right)\Bigg] \tag{A.13c}$$
$$+ \frac{1}{2}\sum_{j=i+1}^{N} D_\omega\mathbf{F}^{\mathbf{M}}_{2,(j-k,-j)}\left(\check{\mathbf{q}}_{(j,s)}, \check{\mathbf{q}}_{(k-j,s)}\right)$$
$$+ \frac{1}{2}\sum_{j=i+1}^{N} D_\omega\mathbf{F}^{\mathbf{M}}_{2,(j-k,-j)}\left(\check{\mathbf{q}}_{(j,c)}, \check{\mathbf{q}}_{(k-j,c)}\right) \tag{A.13d}$$

References

[1] L. Shaabani-Ardali, D. Sipp, L. Lesshafft, Time-delayed feedback technique for suppressing instabilities in time-periodic flow, Phys. Rev. Fluids 2 (11) (2017) 113904.

[2] D. Jallas, O. Marquet, D. Fabre, Linear and nonlinear perturbation analysis of the symmetry breaking in time-periodic propulsive wakes, Phys. Rev. E 95 (6) (2017) 063111.

[3] M. Krack, J. Gross, Harmonic Balance for Nonlinear Vibration Problems, Springer, 2019.

[4] V. Mantič-Lugo, C. Arratia, F. Gallaire, Self-consistent mean flow description of the nonlinear saturation of the vortex shedding in the cylinder wake, Phys. Rev. Lett. 113 (8) (2014) 084501.

[5] V. Mantič-Lugo, C. Arratia, F. Gallaire, A self-consistent model for the saturation dynamics of the vortex shedding around the mean flow in the unstable cylinder wake, Phys. Fluids 27 (2015) 074103.

[6] P. Meliga, Harmonics generation and the mechanics of saturation in flow over an open cavity: a second-order self-consistent description, J. Fluid Mech. 826 (2017) 503–521.

[7] D. Fabre, V. Citro, D.F. Sabino, P. Bonnefis, J. Sierra, F. Giannetti, M. Pigou, A practical review on linear and nonlinear global approaches to flow instabilities, Appl. Mech. Rev. 70 (6) (2019) 060802.

[8] A. Fani, V. Citro, F. Giannetti, F. Auteri, Computation of the bluff-body sound generation by a self-consistent mean flow formulation, Phys. Fluids 30 (2018) 036102.

[9] K.C. Hall, J.P. Thomas, W.S. Clark, Computation of unsteady nonlinear flows in cascades using a harmonic balance technique, AIAA J. 40 (5) (2002) 879–886.
[10] D.J. Mavriplis, Z. Yang, Time spectral method for periodic and quasi-periodic unsteady computations on unstructured meshes, Math. Model. Natl. Phenom. 6 (3) (2011) 213–236.
[11] K. Ekici, K.C. Hall, Nonlinear analysis of unsteady flows in multistage turbomachines using harmonic balance, AIAA J. 45 (5) (2007) 1047–1057.
[12] F. Sicot, G. Dufour, N. Gourdain, A time-domain harmonic balance method for rotor/stator interactions, J. Turbomach. 134 (1) (2012).
[13] I. Gatin, G. Cvijetić, V. Vukčević, H. Jasak, Š. Malenica, Harmonic balance method for nonlinear and viscous free surface flows, Ocean Eng. 157 (2018) 164–179.
[14] W. Yao, S. Marques, A harmonic balance method for nonlinear fluid structure interaction problems, Comput. Struct. 201 (2018) 26–36.
[15] D. Ramezanian, D. Mavriplis, B.R. Ahrabi, An order n log n parallel solver for time-spectral problems, J. Comput. Phys. 411 (2020) 109319.
[16] S.A. Orszag, On the elimination of aliasing in finite-difference schemes by filtering high-wavenumber components, J. Atmos. Sci. 28 (6) (1971) 1074.
[17] M. Parsani, D.I. Ketcheson, W. Deconinck, Optimized explicit runge–kutta schemes for the spectral difference method applied to wave propagation problems, SIAM J. Sci. Comput. 35 (2) (2013) A957–A986.
[18] V. Citro, F. Giannetti, J. Sierra, Optimal explicit runge-kutta methods for compressible navier-stokes equations, Appl. Numer. Math. (2019).
[19] E.J. Kubatko, B.A. Yeager, D.I. Ketcheson, Optimal strong-stability-preserving runge–kutta time discretizations for discontinuous galerkin methods, J. Sci. Comput. 60 (2) (2014) 313–344.
[20] D. Fabre, V. Citro, D. Ferreira Sabino, P. Bonnefis, J. Sierra, F. Giannetti, M. Pigou, A practical review on linear and nonlinear global approaches to flow instabilities, Appl. Mech. Rev. 70 (6) (2018).
[21] E. Tadmor, The exponential accuracy of Fourier and Chebyshev differencing methods, SIAM J. Numer. Anal. 23 (1) (1986) 1–10.
[22] D. Sipp, A. Lebedev, Global stability of base and mean flows: a general approach and its applications to cylinder and open cavity flows, J. Fluid Mech. 593 (2007) 333–358.
[23] D. Canuto, K. Taira, Two-dimensional compressible viscous flow around a circular cylinder, J. Fluid Mech. 785 (2015) 349–371.
[24] G. Carte, J. Dušek, P. Fraunié, Numerical simulation of the mechanisms governing the onset of the bénard–von kármán instability, Int. J. Numer. Methods Fluids 23 (8) (1996) 753–785.
[25] O. Inoue, N. Hatakeyama, Sound generation by a two-dimensional circular cylinder in a uniform flow, J. Fluid Mech. 471 (2002) 285.
[26] J. Sierra, P. Jolivet, F. Giannetti, V. Citro, Adjoint-based sensitivity analysis of periodic orbits by fourier-galerkin method, 440, 2021, p. 110403.
[27] F. Sicot, G. Puigt, M. Montagnac, Block-jacobi implicit algorithms for the time spectral method, AIAA J. 46 (12) (2008) 3080–3089.
[28] V. Citro, P. Luchini, F. Giannetti, F. Auteri, Efficient stabilization and acceleration of numerical simulation of fluid flows by residual recombination, J. Comput. Phys. 344 (2017) 234–246.
[29] S. Nimmagadda, T.D. Economon, J.J. Alonso, C.R. Ilario da Silva, Robust uniform time sampling approach for the harmonic balance method, in: 46th AIAA Fluid Dynamics Conference, 2016, p. 3966.
[30] N.L. Mundis, D.J. Mavriplis, Toward an optimal solver for time-spectral fluid-dynamic and aeroelastic solutions on unstructured meshes, J. Comput. Phys. 345 (2017) 132–161.
[31] S. Antheaume, C. Corre, Implicit time spectral method for periodic incompressible flows, AIAA J. 49 (4) (2011) 791–805.
[32] J. Moulin, On the Flutter Bifurcation in Laminar Flows: Linear and Nonlinear Modal Methods (Ph.D. thesis), Institut polytechnique de Paris, 2020.
[33] R. Henrywood, A. Agarwal, The aeroacoustics of a steam kettle, Phys. Fluids 25 (10) (2013) 107101.
[34] D. Fabre, P. Bonnefis, F. Charru, S. Russo, V. Citro, F. Giannetti, P. Luchini, Application of global stability approaches to whistling jets and wind instruments, in: International Symposium on Musical Acoustics (ISMA), Le Mans, France, 2014, pp. 7–12.
[35] R. Longobardi, D. Fabre, P. Bonnefis, V. Citro, F. Giannetti, P. Luchini, Studying sound production in the hole-tone configuration using compressible and incompressible global stability analyses, in: IUTAM Symposium on Critical Flow Dynamics Involving Moving/Deformable Structures with Design Applications, 2018, pp. 18–22.
[36] C. Nana, D. Marx, C. Prax, V. Fortuné, The perturbed low Mach number approximation for the aeroacoustic computation of anisothermal flows, in: Proceedings of the Acoustics 2012 Nantes Conference, 2012, pp. 1285–1290.
[37] P. Cvitanović, Invariant measurement of strange sets in terms of cycles, Phys. Rev. Lett. 61 (24) (1988) 2729.
[38] P. Cvitanovic, R. Artuso, R. Mainieri, G. Tanner, G. Vattay, N. Whelan, A. Wirzba, Chaos: Classical and Quantum, Vol. 69, Niels Bohr Institute, Copenhagen 2005, 2005, ChaosBook.Org.